energies

MDPI

Article

Fluorocarbon Interfacial Modifier: Wettability Alteration in Reservoir Rocks for Enhanced Oil Recovery and Field Application

Ruiyang Liu [1], Huabin Li [2,*], Zhe Li [3,4], Xudong Yu [1], Lide He [1], Xutong Guo [2], Feng Zhao [1], Huaqiang Shi [3,4] and Wenzhao Sun [2]

[1] College of Materials and Chemistry & Chemical Engineering, Chengdu University of Technology, Chengdu 610059, China
[2] College of Energy, Chengdu University of Technology, Chengdu 610059, China
[3] Oil & Gas Technology Research Institute Changqing Oilfield Company, Xi'an 710021, China
[4] Low Permeability Oil and Gas Field Exploration and Development of the National Engineering Laboratory, Xi'an 710021, China
* Correspondence: lihuab1111@163.com

Abstract

The peripheral reservoirs of the Daqing Oilfield exhibit low permeability and partial heterogeneity, resulting in a rapid injection pressure increase, limited sweep efficiency, and significant residual oil retention. To enhance recovery, this study synthesized a fluorocarbon siloxane (FHB) via free radical addition for rock surface wettability modification. At a concentration of 0.1 wt%, FHB increased water and oil contact angles to 136° and 117°, respectively, at 60 °C. Fourier transform infrared spectroscopy, thermogravimetric analysis, and aging tests confirmed stable hydrophobic/oleophobic properties through chemical bonding to the rock. Furthermore, the low surface energy FHB significantly reduced adhesion work and decreased oil-water interfacial tension from 27 mN/m to 0.55 mN/m, thereby improving fluid transport in pore throats and promoting residual oil mobilization. Core flooding experiments resulted in an increase in total recovery by 11%, with low-field NMR analysis confirming reduced oil saturation across various pore sizes. A field trial in a production well in Daqing Oilfield successfully increased output from 3.1 t/d to 4.9 t/d, validating the efficacy of this strategy under real reservoir conditions—representing the first successful field application of a fluorocarbon-based modifier for wettability alteration and oil production enhancement in China. This study provides valuable experimental data and a practical framework for implementing chemical-enhanced recovery.

Keywords: fluorocarbon compounds; low-permeability reservoirs; wettability alteration; core flooding; enhanced oil recovery

check for updates

Academic Editor: Hossein Hamidi

Received: 28 September 2025
Revised: 8 October 2025
Accepted: 14 October 2025
Published: 16 October 2025

Citation: Liu, R.; Li, H.; Li, Z.; Yu, X.; He, L.; Guo, X.; Zhao, F.; Shi, H.; Sun, W. Fluorocarbon Interfacial Modifier: Wettability Alteration in Reservoir Rocks for Enhanced Oil Recovery and Field Application. *Energies* **2025**, *18*, 5463. https://doi.org/10.3390/en18205463

Copyright: © 2025 by the authors. Licensee MDPI, Basel, Switzerland. This article is an open access article distributed under the terms and conditions of the Creative Commons Attribution (CC BY) license (https://creativecommons.org/licenses/by/4.0/).

1. Introduction

Against the backdrop of sustained global economic development and continuous population growth, the demand for energy continues to exhibit an upward trend. According to the International Energy Agency's (IEA) World Energy Outlook 2024, although the transition to clean energy is accelerating, the dominance of traditional energy sources remains difficult to displace in the short term. As a crucial component of the global energy mix, the demand for oil is expected to remain at a high level for the foreseeable future [1,2].

However, conventional reservoirs have generally entered a high water-cut stage after long-term intensive development. China's major oilfields boast a recovery factor below

50%, with remaining oil highly dispersed—making effective extraction challenging via traditional water flooding. Meanwhile, low-permeability reservoirs have emerged as critical replacement resources: China's proven reserves in such reservoirs exceed 20 billion tons, accounting for over 65% of onshore petroleum reserves, with the Ordos Basin alone holding several billion tons of low-permeability oil reserves [3,4]. Nevertheless, these reservoirs (permeabilities typically < 50 mD) face a stark "abundant reserves but low extraction efficiency" dilemma: per-well daily production is less than one-fifth of conventional reservoirs, while essential technologies like fracturing and advanced water injection raise development costs by 2–3 times. More critically, ultra-low permeability reservoir heterogeneity creates complex flow pathways, deviating from conventional Darcy flow. Water injection efficiency drops over 30% versus theoretical values, further intensifying economic and technical hurdles in resource development [5,6]. This contradiction limits efficient petroleum utilization and challenges energy supply stability, making enhancing low-permeability reservoir recovery and exploring targeted technologies urgent priorities for the petroleum industry.

To address low injectivity, poor retention, and high costs in low-permeability reservoirs, current development methods primarily include chemical flooding, physical stimulation, and gas injection. Chemical flooding enhances recovery by injecting surfactants or polymers to improve oil-water flow conditions [7]. Physical stimulation (e.g., fracturing, horizontal well development) effectively boosts permeability and fluid mobility, while gas injection (e.g., CO_2 flooding) improves recovery by supplementing reservoir energy and modifying fluid properties [8]. Recent advances in refined waterflooding (e.g., ion-matched waterflooding, micro-nano bubble flooding) also show potential in expanding sweep efficiency [9]. Despite these gains, existing methods still suffer from limited recovery enhancement and short production uplift periods.

To overcome the limitations of the aforementioned methods, reservoir wettability modification has emerged as a viable strategy for EOR, drawing significant research interest. Fluorocarbon-based interfacial modifiers, as a novel material class, have gained growing attention. In fluorocarbon molecular structures, the C–F bond (485 kJ/mol bond energy, far higher than 414 kJ/mol of C–H) and short length (0.138 nm) impart exceptional chemical inertness and thermal stability. These properties enable fluorocarbon agents to retain activity under harsh conditions (high temperature, e.g., deep reservoirs; high salinity; strong acidity/alkalinity), preventing performance degradation common in conventional surfactants from environmental deactivation. Moreover, the low polarity (hydrophobic and oleophobic) of fluorocarbon chains results in minimal affinity for aqueous and oil phases, facilitating high-density adsorption layer formation at the oil–water interface—providing a theoretical basis for improving rock surface/interfacial properties and enhancing oil recovery [10]. Liu et al. [11] showed fluoride FC-1 reduced oil–water interfacial tension (6.072 to 2.04 mN/m) while forming a low-surface-energy rock coating, shifting wettability to hydrophobic/oleophobic, lowering injection pressure and boosting recovery. Al-Amodi et al. [12] combined fluorinated surfactants (FS-50, FS-61) with HPAM in carbonate core floods, achieving 42% additional oil recovery and significant interfacial tension reduction (7 to 0.001 mN/m). Zhao et al. [4] reported fluorinated-chain modification of nano-SiO_2 created micro/nano roughness on reservoir rocks, inducing a "lotus leaf effect" to enhance hydrophobicity and oleophobicity, reducing injection pressure and boosting production in low-permeability reservoirs. These studies indicate strong potential for fluorinated agents in low-permeability reservoirs, particularly in improving water injection efficiency and recovery. However, research and application of fluorocarbon interfacial modifiers in low-permeability reservoirs are still in the initial exploratory stage. Their functional effects and optimization methods require supplementation with extensive experimental

data, and field application cases remain relatively scarce. Notably, offshore field trials (e.g., Prirazlomnaya platform) have emphasized real-time monitoring of core parameters (e.g., bottomhole pressure, wellhead temperature) to ensure reliable field validation, which can provide methodological references for onshore low-permeability reservoir tests [13].

In this study, a fluorocarbon interfacial modifier, perfluorododecyltrimethoxysilane (temporarily referred to as FHB), was synthesized and evaluated for its performance as an injection solution system in EOR applications. The chemical bonding and effects of FHB on rock surfaces were analyzed using FT-IR, XPS, SEM, EDS, and contact angle measurements, confirming its stability. The reduction in capillary resistance within pore throats and the adhesion work of liquids on low-surface-energy cores were investigated, while the decrease in interfacial tension (IFT) was measured to validate EOR feasibility. Core flooding experiments were conducted to systematically determine changes in oil recovery and permeability, assessing the system's improvement of oil-water flow behavior. Finally, a field trial was carried out in the Daqing Oilfield, where a production well was selected to evaluate the engineering application effectiveness, providing practical case support for the broader implementation of this research achievement.

2. Materials and Methods

2.1. Materials

Perfluorododecyl iodide ($C_{12}F_{25}I$), vinyltrimethoxysilane (VTMS), radical initiator 2,2′-azobis (2-methylpropionitrile) (abbreviated as AIBN), and hydroquinone were employed to synthesize FHB. Tetrahydrofuran (THF) served as the solvent. Sodium dodecylbenzenesulfonate (SDBS), ethanol, and acetic acid acted as cosolvents to formulate the FHB above into an injection solution for modifying reservoir surface properties. Deionized water (Resistivity > 18 MΩ·cm) and n-hexadecane were utilized for measuring rock surface free energy and adhesion work. All reagents were purchased from Macklin Biochemical Co., Ltd. (Shanghai, China) with analytical purity.

The crude oil sample was collected from a block in the Daqing Oilfield, exhibiting a viscosity of 40 mPa·s and a density of 0.861 g/cm^3 at the reservoir temperature of 55 °C. The formation water used in experiments was sourced from the Daqing Oilfield, with an average salinity of 2536 mg/L and a density of 1.013 g/cm^3. The ionic composition of the formation water is detailed in Table 1. Natural sandstone cores extracted from the target oil layer corresponding to the pilot well group in the Daqing Oilfield were employed, with dimensions of 2.5 cm in diameter and 5 cm in length. To ensure both representativeness and consistency while minimizing the influence of inherent heterogeneity, all cores were rigorously selected based on closely matched petrophysical properties characteristic of the reservoir. The selection criteria required a porosity of 14–20% and an air permeability of 5–50 mD. Only cores meeting these specific criteria were used for the subsequent experiments. Contact angles were measured using core plugs sectioned from these preselected cores.

Table 1. Ionic composition and salinity of formation water.

Ionic Composition (mg/L)							Salinity (mg/L)
Na^+	K^+	Mg^{2+}	Ca^{2+}	Cl^-	SO_4^{2-}	HCO_3^-	2536.1
897.8		5.6	28.9	1233.7	19.2	350.9	

2.2. Synthesis of FHB

In a dry reactor under N_2 atmosphere, $C_{12}F_{25}I$, VTMS, AIBN, and THF were added. The mixture was gradually heated to 75 °C with stirring for 30 min, during which AIBN began to decompose (chain initiation stage). The temperature was then increased to 105 °C

at a rate of 1 °C/min, and the reaction was stirred for 4 h (chain propagation stage). Samples were taken hourly, and the reaction progress was monitored by gas chromatography. The reaction was considered complete when the peak area of the starting material decreased to <5% of its initial value. Finally, for termination and purification, the mixture was cooled below 50 °C, followed by the addition of hydroquinone (radical quencher). THF was recovered (40 °C, 0.1 MPa), and unreacted PF was collected via reduced-pressure distillation (80 °C, 0.05 MPa). The product was further purified by column chromatography to obtain the FHB product as a colorless liquid with a purity exceeding 98% (see synthetic route scheme in Figure 1).

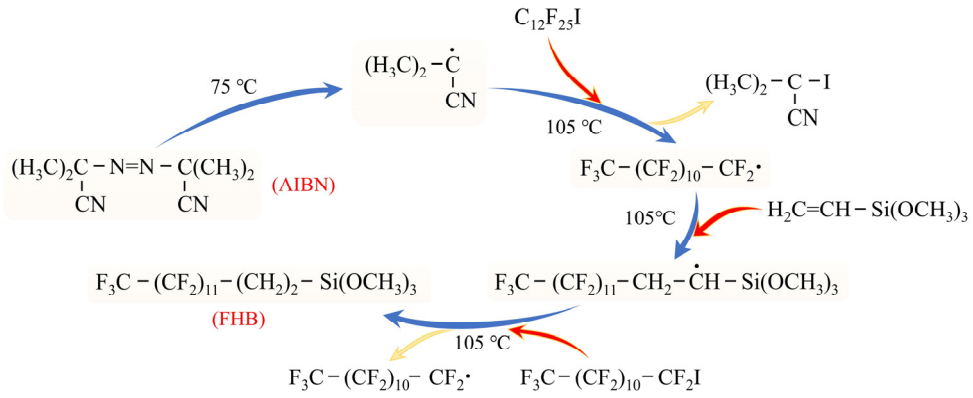


Figure 1. Synthetic route of FHB.

2.3. Preparation of FHB Solution

To prepare the fluorocarbon compound FHB as an injection solution, follow the steps below: First, dissolve a specified amount of SDBS in formation water at 50 °C under continuous stirring. The solution will transition from a grayish-white translucent state to transparent, indicating complete dissolution of SDBS. Next, cool the mixture to room temperature. Sequentially add ethanol and a small amount of acetic acid, ensuring thorough mixing of all components. Finally, incorporate FHB, stir until homogeneous, and seal the solution for further use.

2.4. Characterization of FHB Modification Effects

X-ray photoelectron spectroscopy (XPS, K-Alpha, Thermo Fisher, Waltham, MA, USA) was employed to precisely detect the types and contents of elements in the extremely thin layer (10 nm) on the core surface, and the formation of chemical bonds was determined based on binding energy shifts. Changes in functional groups on the core surface before and after FHB modification were analyzed using Fourier transform infrared spectroscopy (FT-IR, IRTracer-100, Shimadzu, Kyoto, Japan). After confirming the successful modification of the core surface by FHB, wetting contact angles were measured to evaluate the hydrophobic and oleophobic properties of the modified surface (DSA255, KRÜSS, Hamburg, Germany). Specifically, the prepared FHB solution was placed at graded temperature levels for 5 days. The core surface was then treated with the solution at corresponding temperatures for 12 h, followed by washing and drying before contact angle measurement. This procedure provided preliminary insight into the thermal stability of the FHB system and its effectiveness on the core. Similarly, after treating the core with the FHB solution, it was aged for 120 days in formation water at 55 °C under pressurized (5 MPa) and sealed conditions. Contact angles were periodically measured to preliminarily assess the anti-aging performance of the FHB treatment under simulated reservoir conditions. For each

set of contact angle data, five measurements were taken at different locations on the core slice to obtain representative wettability results, with a relative uncertainty of less than 2%.

2.5. Measurement of Rock Surface Free Energy

The wettability alteration in core surfaces relies on the low surface energy fluorinated modifier FHB. To quantify changes in surface free energy before and after FHB treatment, the Owens two-liquid method was employed [14,15]. This approach is grounded in surface energy decomposition theory, dividing the solid surface free energy (γ_S) into a polar component (γ_S^p) and a dispersive component (γ_S^d) (as expressed in Equation (1)):

$$\gamma_S = \gamma_S^p + \gamma_S^d \tag{1}$$

The surface free energy components can be determined by measuring the contact angles (θ) of two probe liquids with known surface tension components (polar and dispersive) on the solid surface. These values (γ_L^p and γ_L^d) are then substituted into Equations (2) and (3) to solve the simultaneous equations. The derived surface free energy components exhibit a relative uncertainty of ±2%, propagated from contact angle measurements.

$$\gamma_L(1+\cos\theta) = 2\left(\sqrt{\gamma_S^d\gamma_L^d} + \sqrt{\gamma_S^p\gamma_L^p}\right) \tag{2}$$

$$\gamma_L = \gamma_L^p + \gamma_L^d \tag{3}$$

The total surface tension of the liquids (γ_L) comprises both polar (γ_L^p) and dispersive (γ_L^d) components. For deionized water: γ_{L1} = 72.8 mN/m, γ_{L1}^p = 51.0 mN/m, γ_{L1}^d = 21.8 mN/m; for n-hexadecane: γ_{L2} = 27.6 mN/m, γ_{L2}^p = 0 mN/m, γ_{L2}^d = 27.6 mN/m [16].

Based on the contact angles of deionized water and n-hexadecane on modified core surfaces, the adhesion work between liquids and core surfaces can be calculated using the Young-Dupré equation (Equation (4)) [17]. This provides preliminary analysis of how hydrophobicity and oleophobicity reduce liquid adhesion resistance:

$$W_{SL} = \gamma_L(\cos\theta + 1) \tag{4}$$

In Equation (4): W_{SL} represents the adhesion work at the liquid-solid interface (mJ/m^2); γ_L denotes the surface tension of the liquid (mN/m); θ is the contact angle between the liquid and solid surface (°). The relative uncertainty was ±2% in adhesion work values.

2.6. Measurement of Oil-Water IFT Reduction

To verify that FHB solution can not only alter the surface properties of rocks but also enhance oil recovery through other mechanisms—such as reducing oil-water IFT, softening residual oil, and improving mobility ratio, thereby promoting the mobilization of residual oil—this study further measured the changes in IFT using the spinning drop method (CNGTX700, Shengwei Tech., Beijing, China). The test liquid and oil droplets were loaded into the sample cell. Under rotation, the droplet formed an elongated shape due to the combined effects of gravity, centrifugal force, and IFT. The oil-water IFT value was calculated using data including the oil-water density difference, rotational angular velocity, and cylindrical droplet radius [18].

All reported IFT values represent equilibrium measurements obtained after prolonged rotation until droplet morphology stabilized. Each data point is the average of three replicates, with a relative uncertainty of ±2%.

2.7. Oil Displacement Experiments

The core flooding comprised five main stages: water saturation, oil saturation, primary water flooding, FHB solution injection, and secondary water flooding. During water saturation, cores were first placed under vacuum conditions followed by water injection via displacement apparatus to ensure full saturation (HKY-1, Hai'an Pet. Res. Instrum., Nantong, China). Injection pressure and effluent flow rate were continuously monitored during water flooding and FHB injection to calculate fluid permeability changes. All core flooding tests were conducted in triplicate (n = 3) for each experimental condition to ensure the reliability and statistical significance of the results. The data presented in the relevant tables are reported as the mean value ± standard deviation. Experimental procedures followed Chinese national standards: "Practices for Core Analysis (GB/T 29172-2012)" [19] and "Test Method for Two-Phase Relative Permeability in Rock (GB/T 28912-2012)" [20].

Furthermore, based on our prior research, the presence of bound water films in core pores impedes fluid transport. Therefore, a set of gas displacement experiments was designed to measure the water film thickness in pore throats [21], aiming to investigate the improvement effect of FHB on pore seepage. After saturating the core with formation water, gas displacement was first performed to measure the water film thickness under blank control conditions. Then, FHB solution was injected and allowed sufficient reaction, followed by re-saturating with formation water. Subsequent gas displacement was conducted again to measure the reduction in water film thickness after modification. The water film calculation was based on Equations (5) and (6), with a relative uncertainty of 1%.

$$S = 7 \times 10^3 \varphi \sqrt{\frac{\varphi}{K}} \tag{5}$$

$$d = \frac{(V_p - V_w)}{V_R \times S} \times 10^7 \tag{6}$$

The relevant parameters include porosity (φ, dimensionless), permeability (K, mD), specific surface area (S, cm^2/cm^3), cumulative displaced water volume at the outlet (V_w, cm^3), pore volume (V_p, cm^3), and core volume (V_R, cm^3); water film thickness (d, nm).

2.8. Low-Field Nuclear Magnetic Resonance Analysis

Low-field nuclear magnetic resonance (LF-NMR, MesoMR23-060H-I, Niumag, Suzhou, China) technology precisely characterizes oil-water distribution in rock pores by detecting the relaxation behavior of hydrogen nuclei (^1H) in a magnetic field. The core principle relies on distinct relaxation properties of hydrogen nuclei in oil versus water molecules, enabling signal separation via pulse sequences. To exclusively measure oil distribution, formation water containing 2.5 wt% $MnCl_2$ was used to shorten the aqueous phase relaxation time [22]. Fluid relaxation times (T_2) in pores involve three mechanisms: surface relaxation (T_{2s}), bulk relaxation (T_{2b}) and diffusion relaxation (T_{2d}) [23]. These are governed by Equation (7):

$$\frac{1}{T_2} = \frac{1}{T_{2s}} + \frac{1}{T_{2b}} + \frac{1}{T_{2d}} \tag{7}$$

T_{2s} represents the transverse relaxation time dominated by surface relaxation, where energy dissipation occurs through fluid molecule collisions with pore walls. This parameter directly reflects pore size distribution. T_{2b} denotes bulk relaxation (or free relaxation), characterizing the intrinsic relaxation of fluid molecules in unconfined bulk environments (where container effects are negligible). In microscale rock pores, T_{2b} significantly exceeds T_2, rendering $1/T_{2b} \approx 0$. T_{2d} arises from diffusion relaxation, describing phase dispersion caused by molecular diffusion in magnetic field inhomogeneities. Under LF-NMR condi-

tions (minimal field gradients and short recovery times), T_{2d} contributions are negligible. Consequently, the observed T_2 is primarily governed by T_{2s}, which correlates with the specific surface area of pores as expressed in Equation (8):

$$\frac{1}{T_2} \approx \frac{1}{T_{2s}} = \rho_2 \left(\frac{S}{V} \right) \tag{8}$$

In Equation (8), ρ_2 denotes the surface relaxivity for T_2 (μm/ms); S/V represents the specific surface area of pores (μm^{-1}). For idealized spherical or cylindrical pore geometries, the relationship between specific surface area and pore radius is given by Equation (9):

$$\frac{S}{V} = \frac{F_s}{r_c} \tag{9}$$

where F_s is the shape factor. For cylindrical pores, $F_s = 2$; r_c refers to the pore radius, μm. Thus, the relationship between T_2 and r_c can be summarized as follows:

$$T_2 = \frac{r_c}{\rho_2 F_s} \tag{10}$$

Rearranging gives the r_c calculation formula (Equation (11)):

$$r_c = 2\rho_2 T_2 = CT_2 \tag{11}$$

In the formula, C is a conversion coefficient (ms/μm). Based on the selected core type (tight sandstone cores from the southern Songliao Basin) in the experiment and the results of mercury intrusion experiments from the literature [24], this calibrated value of C is set to 0.04 that is:

$$r_c = 0.04T_2 \tag{12}$$

2.9. Field Trial

Based on the promising results from laboratory experiments, a field trial was conducted in a production well from the Daqing Oilfield. The operational procedure involved the direct tubing injection of a 2 wt% FHB solution alternated with formation water, utilizing a designed huff-and-puff process (see Table 2 for specific parameters). Following the chemical injection, a substantial volume of formation water was injected to displace the chemical slug deep into the formation and prevent its retention within the tubing. The well was subsequently shut in for 2 days to allow sufficient reaction time between FHB and the reservoir rock. Afterwards, the well was returned to normal water-flooding operations. The subsequent monitoring of oil production rate and water cut confirmed the effective engineering application and performance of the FHB system for enhancing oil recovery.

Table 2. Implementation details of FHB huff-and-puff process in field trials.

Total FHB Injection (m^3)	Primary FHB Injection (m^3)	Primary Water Injection (m^3)	Secondary FHB Injection (m^3)	Secondary Water Injection (m^3)	Tertiary FHB Injection (m^3)	Tertiary Water Injection (m^3)	Daily Water Injection During Production (m^3)
3	1	120	1	250	1	100	30

3. Results and Discussion

3.1. Interfacial Modification Characterization

The structure of the synthesized FHB was first analyzed by ^1H and ^{13}C nuclear magnetic resonance (NMR, AVANCE NEO 400, Bruker, Karlsruhe, Germany) spectroscopy

(solvent: deuterated chloroform; frequency: 400 MHz), as shown in Figure 2a. A strong singlet at a chemical shift (δ) of 3.56 ppm (labeled 'a') is assigned to the hydrogen atoms of the methoxy groups (–OCH_3) linked to the silicon atom in the FHB molecule. The electronegativity of the oxygen atom causes a deshielding effect on the hydrogen nuclei, while the weak electron-donating character of silicon partially counteracts this deshielding, resulting in a chemical shift slightly lower than that of typical alkoxy groups (usually δ 3.5–3.8 ppm). The three methoxy groups are chemically equivalent and exhibit no spin-spin coupling with neighboring non-equivalent hydrogen nuclei, resulting in a well-defined singlet. The peak at δ = 2.11 ppm (b) is attributed to the hydrogen atoms of the fluoroproximate methylene group (–CH_2–CF_2–). The strong electron-withdrawing inductive effect of the fluorine atoms deshields the hydrogen nuclei, causing a downfield shift relative to a typical methylene group. This peak has a coupling constant (J-value) of 18.4 Hz, primarily resulting from ^{19}F-^{1}H spin-spin coupling with the adjacent –CF_2– fluorine atoms. The increased length of the fluorocarbon chain and greater steric hindrance weaken this coupling interaction (J < 20 Hz). The triplet at δ 1.55 ppm (c) corresponds to the hydrogen atoms of the silaproximate methylene group (–CH_2–Si–). This methylene group is adjacent to a methylene group containing two equivalent hydrogen nuclei, leading to splitting into a triplet with a J-value of 6.8 Hz, consistent with the characteristic H–H coupling between methylene groups [25,26].

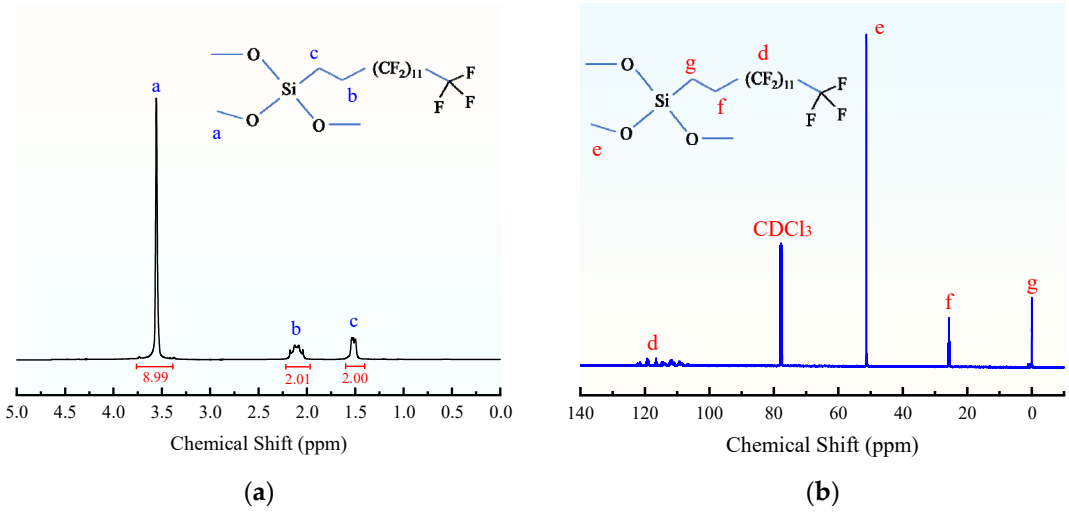


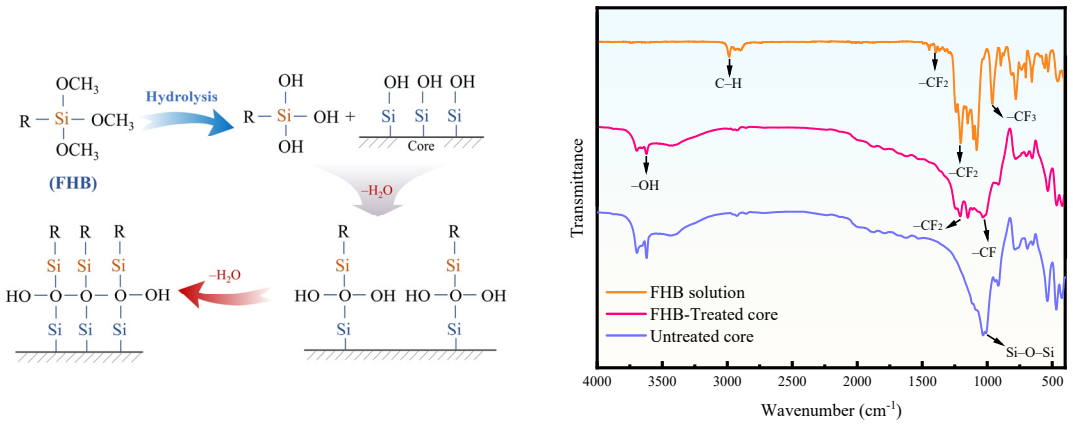
Figure 2. NMR characterization of the synthesized FHB product: (**a**) ^{1}H NMR spectrum of FHB; (**b**) ^{13}C NMR spectrum of FHB. Key proton and carbon assignments are labeled, confirming the successful formation of the target molecular structure.

Integration of the three signal sets yielded a peak area ratio of approximately 9:2:2, which matches the theoretical ratio of the three types of hydrogen atoms in the FHB molecule (methoxy hydrogens: 9; fluoroproximate methylene hydrogens: 2; silaproximate methylene hydrogens: 2).

In the ^{13}C NMR spectrum (Figure 2b), the signal at δ = 77 ppm corresponds to the solvent peak of $CDCl_3$, which appears as a triplet due to spin-spin coupling with the deuterium nuclei. The multiple peaks in the range of 100–130 ppm are attributed to the carbon atoms in the perfluoroalkyl chain. The strong electron-withdrawing effect and spin-spin coupling from multiple fluorine atoms result in complex splitting patterns for these signals. The singlet at δ = 51.3 ppm is characteristic of the –O–CH_3 carbon. The electronegativity of the oxygen atom reduces the electron density around this carbon, causing a downfield shift. The peaks at δ = 25.7 ppm and 0 ppm are assigned to the

fluoroproximate and silaproximate carbon atoms, respectively. The carbon atom adjacent to silicon is less influenced by electronegative atoms, resulting in a signal at a higher field (lower δ value). In conclusion, the ^{1}H and ^{13}C NMR spectra collectively confirm the successful synthesis of FHB and adequately reflect its intended structure ($C_{17}H_{13}F_{25}O_3Si$, molecular weight: 828 g/mol). The product is thus suitable for subsequent rock-surface modification reactions.

The FHB was slowly hydrolyzed in a weak acidic solution to expose reactive hydroxyl groups. After being injected into the well, it could undergo dehydration-condensation with hydroxyl groups on the rock surface at reservoir temperature, forming stable chemical bonds (Figure 3a). This process arranged the fluorinated functional groups (R group, refer to $–C_2H_4–C_xF_y$) on the rock surface, imparting excellent hydrophobic and oleophobic properties. This modification promotes the mobilization of residual oil in pore throats, thereby enhancing oil recovery.



(**a**) (**b**)

Figure 3. (**a**) Reaction process between FHB and core surface; (**b**) FT-IR spectra comparison of FHB solution and cores before and after FHB treatment.

FT-IR was employed to characterize the chemical composition of the fluorinated interfacial modifier FHB and to analyze the functional group distribution on the core surface before and after FHB treatment (Figure 3b). The spectra were recorded in the wavenumber range of 4000–400 cm^{-1}. The untreated core sample exhibited a characteristic –OH stretching peak at 3620 cm^{-1}, indicating the presence of hydroxyl groups on the rock surface, which provided potential reaction sites for FHB. After FHB treatment, the intensity of this –OH peak decreased, indirectly confirming the occurrence of a grafting reaction. Pure FHB solution in its molecular form did not show a significant –OH peak, as hydroxyl groups are exposed only after hydrolysis, enabling the reaction with the core surface. In the FHB spectrum, the peaks observed near 1400 cm^{-1} and 1210 cm^{-1} are attributed to the asymmetric and symmetric stretching vibrations of $–CF_2$ groups, respectively, while the stretching peak at 960 cm^{-1} corresponds to $–CF_3$ groups. The untreated core showed a strong Si–O–Si peak at 1050 cm^{-1}, resulting from the silicate framework of the rock matrix. The high intensity of this peak partially overshadowed the relatively weaker $–CF_3$ and $–CF_2$ peaks in the treated core samples.

In conclusion, the FT-IR results not only reflect the successful synthesis of FHB but also reveal clear changes in the surface functional group distribution of the core after modification. The appearance of characteristic fluorocarbon peaks on the treated core surface confirms the successful chemical grafting of FHB onto the rock, leading to an alteration of its surface properties.

To further verify the successful reaction of FHB with the core surface, the samples before and after modification were characterized by XPS. Figure 4 displays the wide-scan survey spectrum and the high-resolution spectra of O_{1s}, Si_{2p}, F_{1s}, and C_{1s} for the core samples. The consistent changes in binding energy and peak intensity collectively indicate that FHB was successfully grafted onto the core surface via chemical bonding.

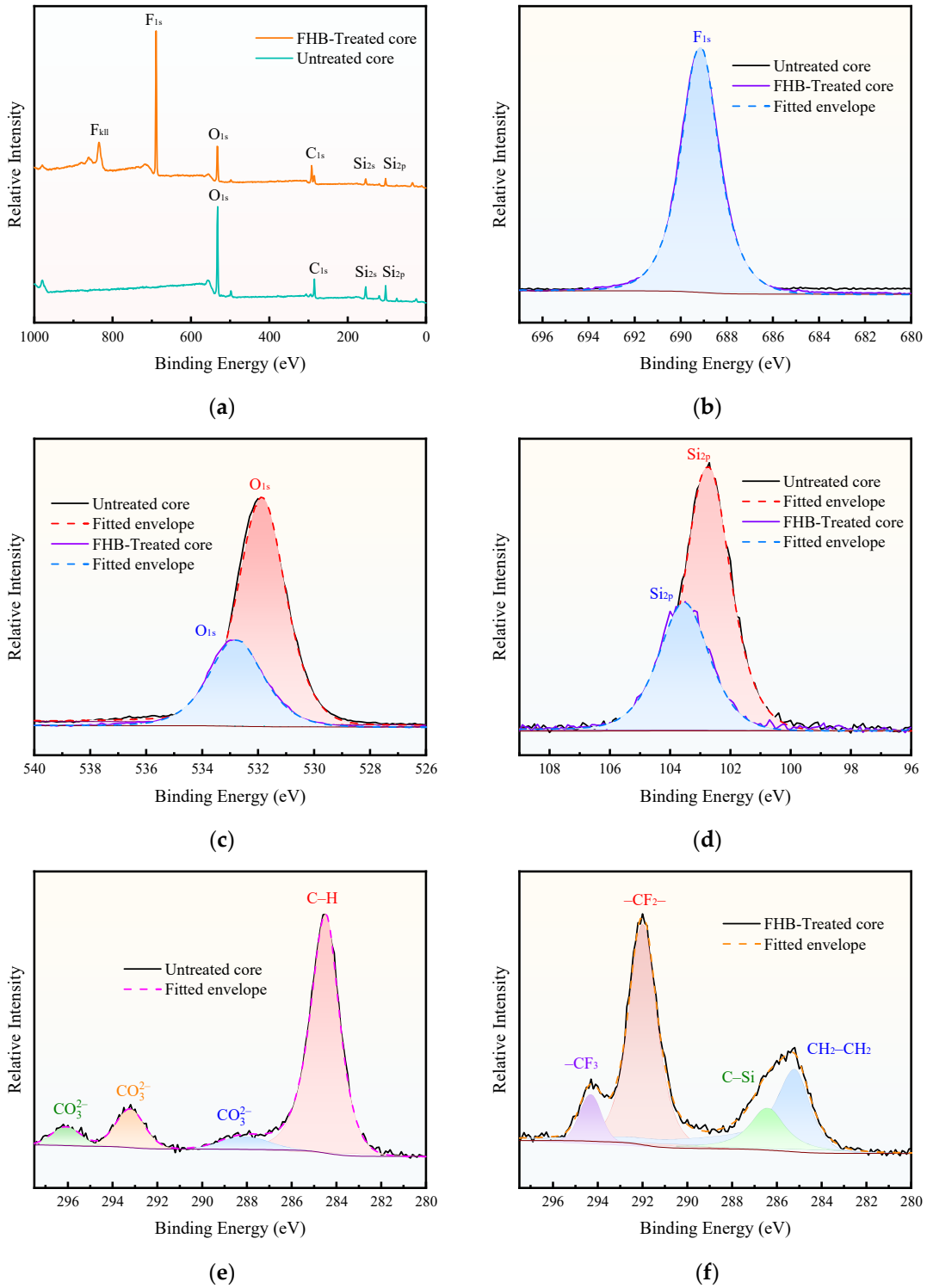


Figure 4. XPS spectra of the core samples before and after FHB modification. (**a**) Survey scan; (**b**) F_{1s}; (**c**) O_{1s}; (**d**) Si_{2p} high-resolution spectra; High-resolution C_{1s} spectra of (**e**) the untreated core and (**f**) the FHB-treated core.

Firstly, no F element signal was detected in the untreated sample, whereas a distinct F_{1s} characteristic peak appeared at 689.11 eV after FHB modification, providing direct evidence for the successful introduction of FHB and the grafting of the fluorocarbon chain (Figure 4b). Changes in the O_{1s} and Si_{2p} spectra (Figure 4c,d) further reveal the bonding mechanism. In the unmodified core, the O_{1s} binding energy was 531.87 eV, primarily attributed to Si–O–Si and surface Si–OH in silicate minerals. After modification, this peak shifted to 532.75 eV, and its intensity significantly decreased, suggesting that the FHB coating produced a shielding effect on the substrate signal and concurrently altered the chemical environment of oxygen. The Si_{2p} spectrum showed a consistent trend: shifting from 102.72 eV (Si–O–Si) in the unmodified state to 103.54 eV after modification, a positive binding energy shift of 0.82 eV. The shifts in the O and Si signals indicate the formation of new chemical bonds between the sandstone surface and the more electronegative modifier (fluorocarbon chain), leading to a decrease in electron density around the silicon atoms. This further supports the formation of new Si–O–Si covalent bonds, consistent with the expected mechanism of a condensation reaction between the hydrolysate of FHB and the surface silanol (Si–OH) groups of the core.

The changes in the C_{1s} spectrum are also significant (see Figure 4e,f). In the unmodified sample, the peaks at 288.04 eV, 293.22 eV, and 296.06 eV originated from partial calcite cement ($CaCO_3$) filling the intergranular spaces of quartz, mainly exhibiting three main CO_3^{2-} peaks and their satellite peaks, while the peak at 284.49 eV was attributed to contaminant C–C/C–H species. After FHB modification, these characteristic mineral peaks almost completely disappeared. Instead, new characteristic peaks for $–CF_2–$ and $–CF_3$ appeared at 291.97 eV and 294.32 eV, respectively. Furthermore, new peaks associated with $–CH_2CH_2–$ and C–Si bonds from the FHB molecule emerged at 285.21 eV and 286.38 eV [15,27]. These results not only confirm the successful grafting of FHB but also indicate that the modification layer is continuous and dense enough to effectively shield the signals from the mineral substrate, forming a stable dual-phobic (hydrophobic/oleophobic) coating on the core surface via chemical bonding. Furthermore, the stable chemical bonding of FHB onto the core surface was corroborated by the static adsorption experiment, which confirmed the formation of a monolayer through chemisorption (see Appendix A for details). This robust and stable interaction aligns well with the XPS findings, collectively demonstrating the effective and durable grafting of the modifier. Such a strong interfacial association suggests great potential for the long-term stability and enhanced oil recovery performance of the treated core under actual oilfield conditions.

The surface morphology of the rock before and after modification was characterized by scanning electron microscopy (SEM, Quanta 250 FEG, FEI, Hillsboro, OR, USA), and the surface elemental composition was determined using energy-dispersive X-ray spectroscopy (EDS). The core samples were thoroughly cleaned with kerosene, ethanol, and distilled water, followed by drying.

SEM images revealed that the unmodified core surface exhibited a relatively smooth and flat morphology (Figure 5a). This is primarily attributed to the fact that the sandstone core is mainly composed of hard mineral grains such as quartz (Mohs hardness 7) and feldspar (Mohs hardness 6–6.5). During the sedimentation process, these minerals underwent prolonged hydrodynamic transport and abrasion, leading to the blunting of grain edges and resulting in a smooth surface. After modification with FHB (Figure 5b), certain changes occurred on the reservoir rock surface, forming micro-nano-scale protrusions. The formation of this structure is likely due to the directional arrangement or aggregation of FHB molecules on the reservoir surface, thereby altering the micro-morphology. It is noteworthy that the formation of this rough surface did not clog the reservoir pores, indicating that the fluorocarbon modifier improved the surface properties while maintaining reservoir

permeability and avoiding formation damage. The combination of this developed surface roughness and the intrinsically low surface energy of the fluorocarbon chains collectively contributed to the enhanced hydrophobic and oleophobic properties of the reservoir rock (Figure 5c).

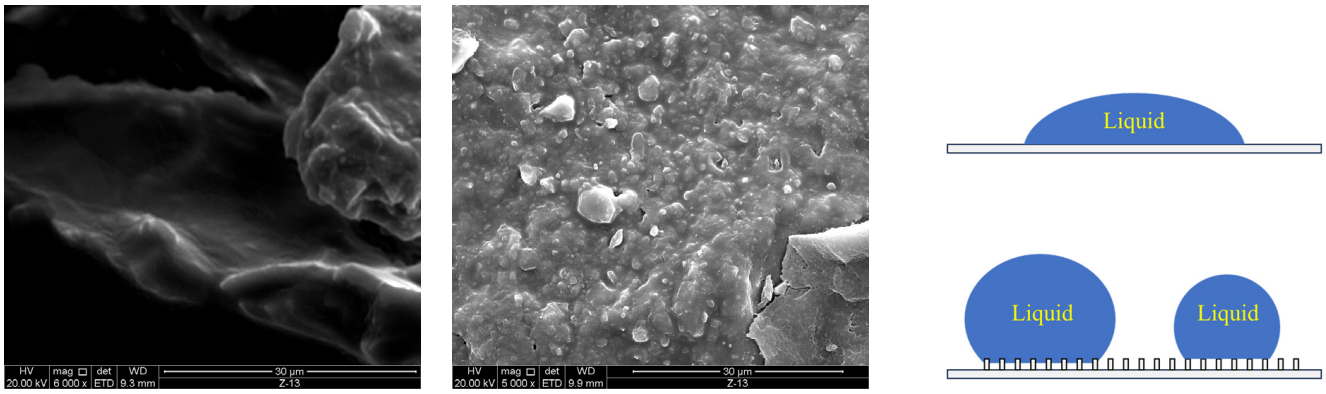


Figure 5. SEM images of core surfaces: (**a**) Untreated core; (**b**) FHB-modified core. (**c**) Schematic diagram of wettability influence by surface roughness and functional group distribution.

Subsequently, the surface roughness of the cores before and after modification was quantitatively characterized using a 3D profilometer (UP-2000, Rtec Instruments, San Jose, CA, USA). Before FHB treatment, both core groups were thoroughly polished with 220-grit sandpaper. One group was immersed in formation water, while the other was reacted with the FHB solution. Quantitative analysis results (Figure 6) showed that the three-dimensional arithmetic mean roughness (Sa) of the unmodified core surface was 25.86 μm. After FHB modification, the average surface roughness increased significantly to 32.73 μm, representing an increase of 26.6%. This indicates that FHB modification effectively constructs a micro-rough structure on the core surface. These micro-nano-scale structures not only avoid significant pore throat blockage—which could cause reservoir damage and reduce production—but also contribute to the excellent hydrophobic and oleophobic properties of the rock surface, thereby serving as one of the mechanisms for enhancing oil recovery.

EDS analysis was performed at corresponding locations on the SEM images to analyze the distribution of FHB on the core surface. For the control group (Figure 7a), i.e., the core surface without FHB treatment, the surface was primarily composed of O, Ca, Si, and C elements. This composition is attributed to the quartz being the main component of the sandstone sample, with pores filled by cementing materials such as calcite. The detected Al and K elements correspond to clay and feldspar minerals. The presence of S and trace Fe elements may originate from residual petroleum sulfonates and the introduction of iron debris from cutting and grinding tools during sample preparation. After FHB modification (Figure 7b), not only did the carbon content on the rock surface increase, but a distinct distribution of F element was also detected, confirming the successful attachment of the fluorinated interfacial modifier to the core. This indicates that the fluorocarbon interfacial modifier formed a stable fluorine-containing coating on the core surface, significantly altering its chemical composition.

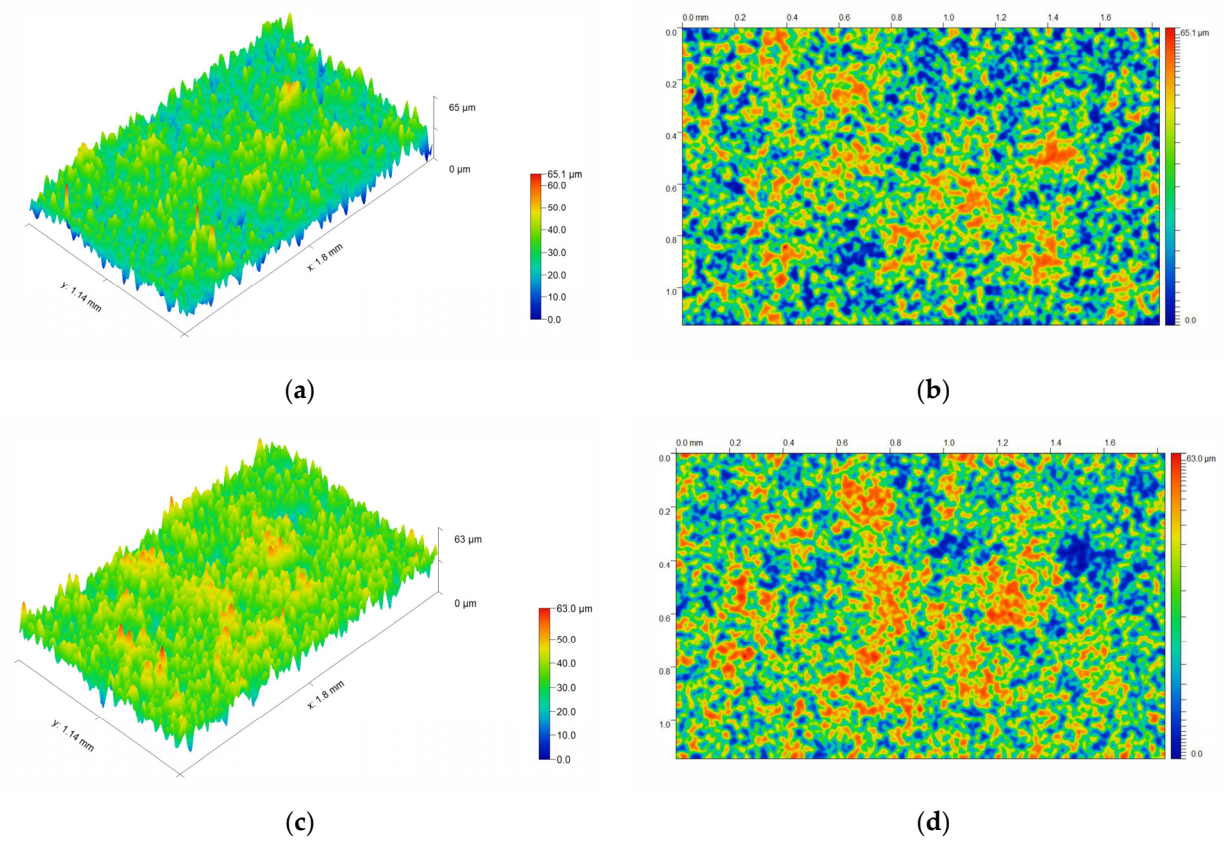


Figure 6. Surface roughness: (**a**) Planar views of the untreated core; (**b**) Three-dimensional views of the untreated core; (**c**) Planar views of the FHB-Treated core; (**d**) Three-dimensional views of the FHB-Treated core.

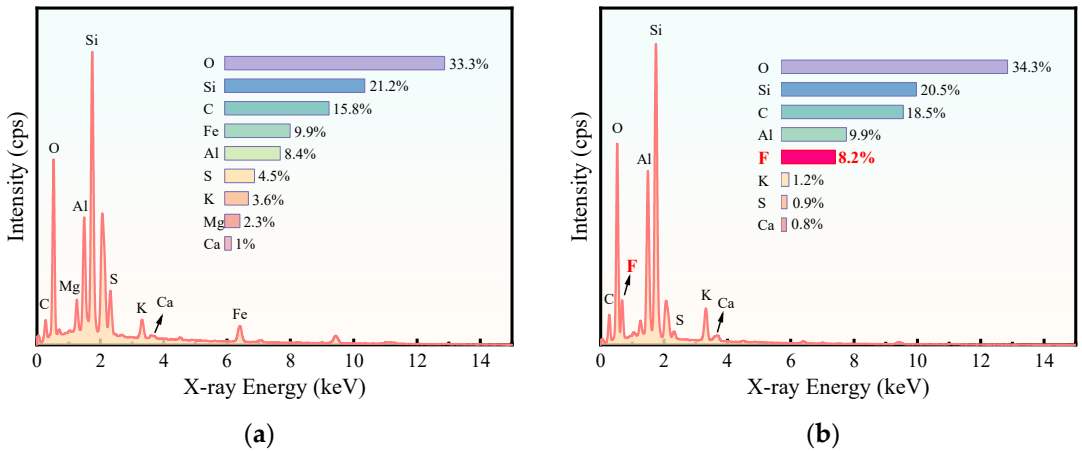


Figure 7. EDS elemental analysis of core surfaces: (**a**) Untreated core; (**b**) FHB-modified core.

3.2. Wettability Alteration Performance

To most directly measure the changes in core surface wettability, the contact angles were measured using oilfield formation water and crude oil. Core surfaces were first treated with FHB solutions at a series of concentration gradients (0.005%, 0.01%, 0.05%, 0.1%, 0.2%, and 0.5%, all by mass fraction) at corresponding temperatures to investigate the effect of FHB on core wettability. The resulting water and oil contact angles are shown in Figures 8 and 9, respectively. The untreated core exhibited contact angles of 0° for both water and oil. As shown in Figure 8, the water contact angle increased rapidly with rising

FHB concentration. The untreated surface was water-wet, but even at a low treatment concentration (0.01 wt%), the surface became hydrophobic (contact angle > 90°). The contact angle continued to rise sharply with further increases in concentration. When the FHB concentration increased from 0.1 wt% to 0.2 wt%, although the contact angle exceeded 150°, reaching the superhydrophobic range, the rate of increase slowed significantly and showed no further improvement with higher concentration. Comparing different solution preparation and treatment temperatures, the contact angle slightly increased as the temperature rose from room temperature to 70 °C. This can be attributed to the improved alignment and exposure of the hydrophobic fluorocarbon chains on the rock surface at higher temperatures, where better functional group coverage is essential for achieving superior hydrophobic and oleophobic properties [28].

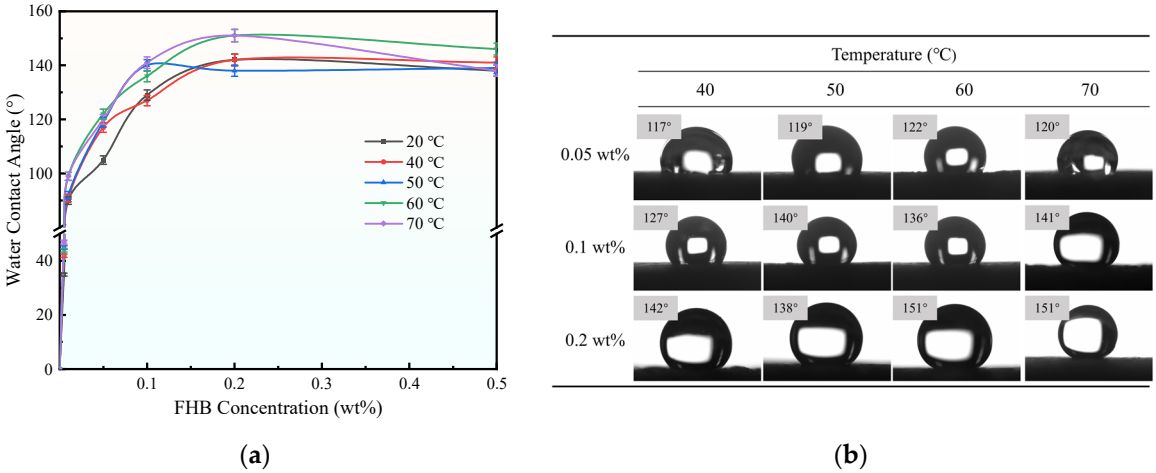


Figure 8. Water wettability alteration by FHB treatment: (**a**) Water contact angle results of cores under different FHB concentrations and treatment temperatures; (**b**) Representative contact angle measurement images.

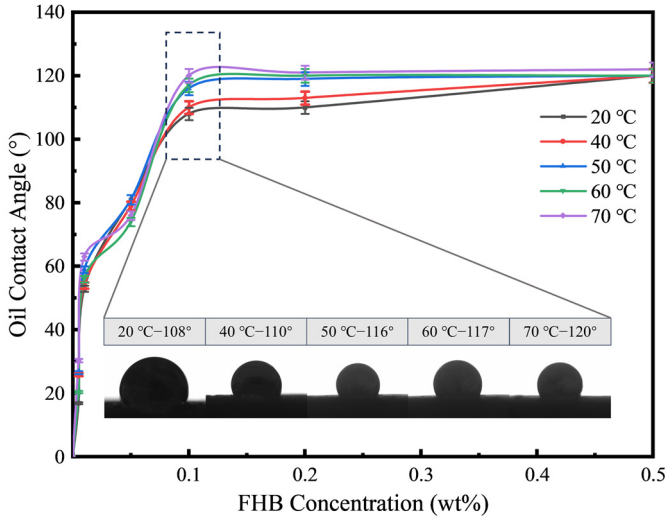


Figure 9. Oil contact angle results and representative images under different FHB concentrations and treatment temperatures.

The oil contact angles of the core samples are shown in Figure 9. When treated with lower FHB concentrations (0.005–0.05 wt%), although the surface wettability was altered, it remained oil-wet (contact angle < 90°). However, when the treatment concentration was increased to 0.1%, the oil contact angle stabilized at approximately 110° across all tested

temperatures, indicating favorable oleophobicity. Further increasing the concentration to 0.2% or 0.5% did not lead to significant improvement in the oleophobic property.

Based on the above results, considering both the wettability alteration effect and practical application costs, a formulation with an FHB solution concentration of 0.1% was selected as the injection solution for further enhanced oil recovery studies. Furthermore, compared to room temperature conditions, the FHB solution stored at reservoir temperature (55 °C) and used to treat the core at this temperature still maintained excellent hydrophobic and oleophobic performances. This demonstrates that the FHB solution possesses good thermal stability, making it suitable for oilfield applications.

Furthermore, thermogravimetric analysis (TGA, TGA/DSC 1, Mettler Toledo, Greifensee, Switzerland) results in Figure 10, the untreated core sample exhibited a minor mass loss of 0.32% over the entire process. This is likely attributable to the thermal decomposition of calcite cement within the core pores, releasing CO_2. For the FHB-treated core sample, the mass remained essentially stable from 40 °C to approximately 300 °C. As the temperature increased further to 400 °C, a significant mass loss began, resulting in a total mass loss of 6.32%. Analysis of the derivative thermogravimetry (DTG) curve indicated that the maximum decomposition rate occurred at around 432 °C, representing the most intense stage of decomposition. Since significant thermal decomposition of the FHB-modified core powder began only after 320 °C, it demonstrates good thermal stability. Compared to the fluorinated betaine-based surfactant (Surfactant-A) and fluorinated amphoteric surfactant (Surfactant-B) reported in the literature [12], which start decomposing at 220 °C and 160 °C, respectively, the chemical bonding of FHB to the core surface (via symmetric Si–O–Si bonds) exhibits superior stability. This enhanced stability is expected to contribute to better anti-aging performance, thereby extending the stable production life of the reservoir. For an excellent fluorinated interfacial modifier like FHB, the long-term retention of altered core surface wettability needs further validation through extended aging experiments.

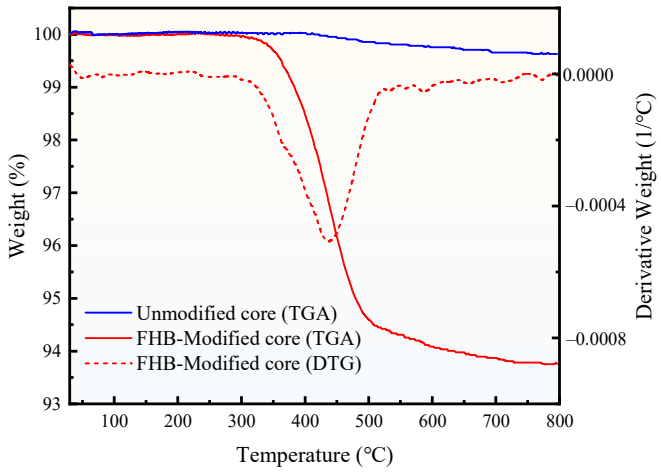


Figure 10. TGA curves of FHB-modified core powder.

Among various wettability modification methods for EOR, many nanoparticles and surfactants can significantly alter the core surface contact angle in the short term, effectively reducing injection pressure and improving fluid flow [29]. However, actual oilfield development involves extended cycles, requiring long-term stability of the altered wettability to prevent reversion to the original water-wet or oil-wet state under heated, prolonged exposure to formation water.

To evaluate the anti-aging performance of the FHB solution and the treated cores, samples treated with 0.1 wt% FHB were aged in formation water at 55 °C for 120 days.

Water and oil contact angles were measured periodically to monitor wettability stability. As shown in Figure 11, the hydrophobic property of the treated core decreased only slightly during the 120-day aging period, from 135° to 124°. The oleophobic property declined to 108° by day 80 (from an initial 118°), after which the decrease slowed, and the surface remained non-oil-wet with an oil contact angle of 103° after 120 days. The sustained hydrophobic and oleophobic properties are primarily attributed to the covalent grafting of fluorocarbon chains onto the core surface, as confirmed by FT-IR and XPS analyses. Compared to traditional surfactants and nanoparticles, which rely on electrostatic adsorption, intermolecular forces, or physical adsorption [30,31], this chemical anchoring offers superior resistance to long-term flushing by heated formation water, demonstrating promising potential for oilfield applications.

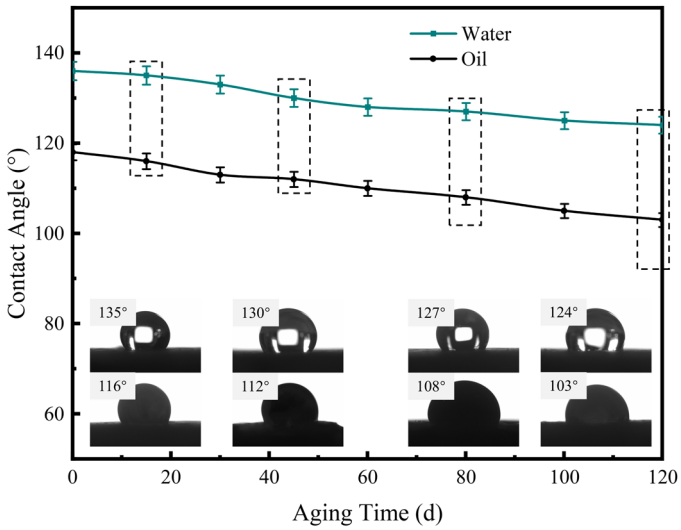


Figure 11. Wettability variation of 0.1 wt% FHB-treated cores during aging experiments.

3.3. Influence of Wettability on Capillary Forces

The relationship between wettability and capillary pressure in core pores is often preliminarily evaluated using spontaneous imbibition tests in glass capillary tubes. CT-1, CT-3, and CT-4 represent capillaries with inner diameters of 0.1 mm, 0.3 mm, and 0.4 mm, respectively. The spontaneous imbibition results of these capillaries in water (dyed red) are shown in Figure 12a. CT-1 demonstrated the strongest water uptake, reaching a height of 38.6 mm, while CT-3 and CT-4 showed sequentially lower heights of 34.9 mm and 19.2 mm, respectively. The oil uptake heights were 42.5 mm, 29.5 mm, and 27.4 mm for CT-1, CT-3, and CT-4, respectively. According to the Young-Laplace equation, the imbibition height is inversely proportional to the capillary radius, which explains the decreasing heights from CT-1 to CT-4.

After cleaning and drying, the capillaries were modified by immersion in an FHB solution and retested (Figure 12b). Due to the induced hydrophobicity, the meniscus shape changed from concave to flat or slightly convex, leading to a sharp reduction in capillary pressure and a significant decrease in liquid uptake. The final uptake heights for water were reduced to 0.6 mm, 1.1 mm, and 2.0 mm for CT-1, CT-3, and CT-4, respectively. This indicates that wettability alteration has a more pronounced effect on the magnitude and direction of capillary forces in smaller pore throats. For oil imbibition, the height in CT-1 became negligible (almost level with the liquid in the vial), CT-3 reached 6.4 mm, while CT-4 showed only a slight reduction in oleophilicity, with an average decrease of 2.3 mm—within the margin of error. Combined with the previous contact angle results, this confirms that the $–CF_2/–CF_3$ groups impart stronger hydrophobicity than oleophobicity.

In larger capillaries like CT-4 (0.4 mm), the slight change in cosθ has minimal impact on oil uptake height.

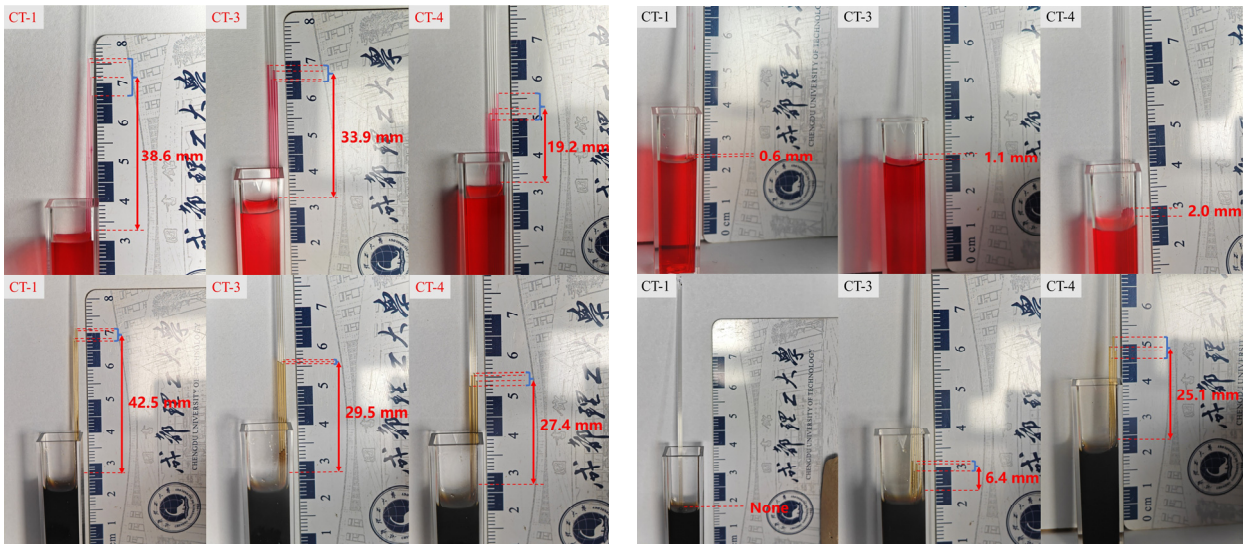


Figure 12. Capillary imbibition tests: (**a**) Liquid imbibition heights for unmodified capillaries; (**b**) Liquid imbibition heights for FHB-modified capillaries.

The sharp decline in capillary-driven water uptake after treatment directly demonstrates how FHB reduces capillary resistance in small pore throats—a key mechanism behind the observed injection pressure drop during core flooding, especially in low-permeability formations featuring numerous fine pores. The induced dual-phobicity promotes more uniform fluid advancement, supporting efficient piston-like displacement. It should be noted, however, that smooth, uniform glass capillaries represent an idealized system. Natural rock pores exhibit complex geometry, surface roughness, and mineralogical heterogeneity, which can lead to non-uniform chemical adsorption and more varied fluid behavior. Nevertheless, the capillary model effectively captures the fundamental wettability-mediated mechanism that underlies fluid redistribution at the pore scale.

In summary, the reduction in capillary resistance observed in smaller capillaries after FHB treatment provides a physical basis for decreasing injection pressure in low-permeability reservoirs. The hydrophobic and oleophobic pore surfaces also promote uniform advancement of both injected water and oil, supporting efficient piston-like displacement and effectively suppressing fingering and water channeling.

3.4. Reduced Fluid Adhesion on Modified Cores

The significant alteration in wettability confirms the successful modification of the core surface properties by FHB, attributed to the treatment with the low-surface-energy fluorinated interfacial modifier. To quantify the change in surface free energy, the Owens two-liquid method was employed, with results shown in Figure 13a. The untreated core, with contact angles of 0° for both water and oil (n-hexadecane), had a calculated surface free energy of 73.2 mN/m. After treatment with a 0.005 wt% FHB solution, the surface free energy decreased sharply to 52.9 mN/m. As the FHB concentration increased within the range of 0.05 wt% to 0.2 wt%, the surface free energy stabilized. At the previously identified optimal concentration of 0.1%, the surface free energy was 2.9 mN/m, representing a remarkable 96% reduction compared to the untreated core.

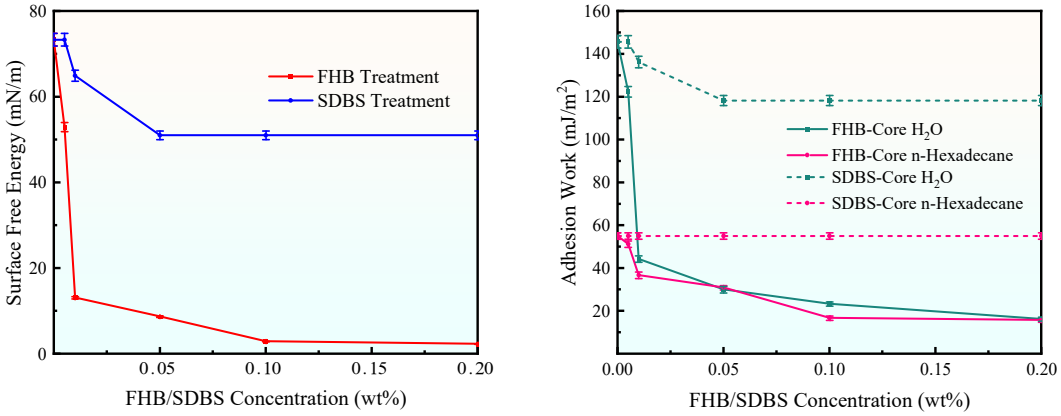


Figure 13. Quantitative surface energy and adhesion work analysis: (**a**) Surface free energy of FHB/SDBS treated cores; (**b**) Adhesion work of liquid on core surface.

Since a small amount of SDBS (<0.1 wt%) was used as a cosolvent in preparing the FHB injection solution, and SDBS itself has been studied and applied in surfactant flooding for EOR [32], controlled experiments were conducted to determine whether the reduction in surface free energy was primarily due to SDBS or FHB. Solutions of SDBS in formation water at various concentrations were prepared separately to treat core surfaces, and the changes in wettability and surface free energy were measured and compared against the FHB results. It was found that SDBS treatment could moderately enhance the hydrophobic character of the core surface but to a limited extent. Crucially, SDBS did not alter the oil contact angle, which remained 0° across all concentrations, indicating a lack of oleophobicity (Table 3). The surface free energy calculation showed that SDBS could only reduce the surface free energy from its original value to 51.0 mN/m, a far smaller reduction than that achieved by the fluorocarbon modifier FHB. Therefore, it is concluded that the superior hydrophobic and oleophobic properties of the FHB-treated core are not primarily attributable to SDBS.

Table 3. Calculated results of surface free energy and adhesion work.

Solution	Concentration (wt%)	Contact Angle (°)		Surface Free Energy (mN/m)	Adhesion Work (mJ/m^2)	
		Deionized Water	n-Hexadecane		Deionized Water	n-Hexadecane
FHB	0	0	0	73.2	145.6	55.0
	0.005	47.1	30.4	52.9	122.3	51.3
	0.01	113.2	70.5	13.1	44.3	36.7
	0.05	125.7	83.0	8.7	30.0	30.9
	0.1	132.8	113.4	2.9	23.3	16.7
	0.2	141.1	115.1	2.3	16.2	15.8
SDBS	0.005	0	0	73.2	145.6	
	0.01	29.5	0	64.9	136.2	
	0.05					55.0
	0.1	51.2	0	51.0	118.4	
	0.2					

Finally, the adhesion work of water and n-hexadecane droplets on the core surface was calculated from the respective contact angles. As seen in Figure 13b, treatment with 0.1 wt% FHB reduced the adhesion work of water by 88% and that of n-hexadecane by 71%. In contrast, SDBS treatment only slightly reduced the adhesion work of water by 27.2 mJ/m^2 and had no effect on the adhesion work of n-hexadecane. This demonstrates that FHB is far more effective at reducing the adhesion work of liquids on the core surface,

thereby promoting their mobility. The grafting of low-surface-energy fluorocarbon chains is identified as the primary mechanism for enhancing oil displacement efficiency.

3.5. IFT Reduction Capability of FHB Solution

The target reservoir formation is relatively tight, with randomly distributed pores and a certain degree of heterogeneity, containing numerous capillaries. When the IFT is low, the capillary resistance opposing oil droplets within the rock pores decreases, making it easier for the oil droplets to be displaced, thereby enhancing the oil displacement efficiency. The strong rock surface modification capability of FHB has been well demonstrated. To further investigate whether its EOR mechanism also involves the ability to reduce the IFT between oil and water phases, a spinning drop tensiometer was used to measure the IFT values in media containing different concentrations of FHB solution at 55 °C.

Figure 14 shows the variation in oil-water IFT in different media. In the formation water medium alone, the IFT is about 27 mN/m. A high IFT not only increases the flow resistance of crude oil within the reservoir, making it difficult to effectively displace oil from the rock pores, but also consequently leads to lower recovery. The results clearly show that while the commonly used surfactant SDBS in water alone can reduce the IFT to 4.51 mN/m—already a good result—the oil-water IFT is further reduced to 0.55 mN/m at the optimal FHB concentration of 0.1 wt%. This represents a total reduction of 98% compared to the value in formation water. Furthermore, the reduction rate is much faster than with the SDBS solution; even at 0.01 wt%, FHB already reduced the IFT to 5.4 mN/m. This indicates that FHB is more efficient at reducing IFT, more effectively improving the flow characteristics of the displacing fluid within the reservoir. This is presumably due to the stronger hydrophobicity of the fluorocarbon chain compared to the hydrocarbon chain of conventional surfactants, allowing faster alignment at the oil-water interface upon contact. This lays the foundation for softening residual oil droplets within the pores and effectively displacing them [33,34].

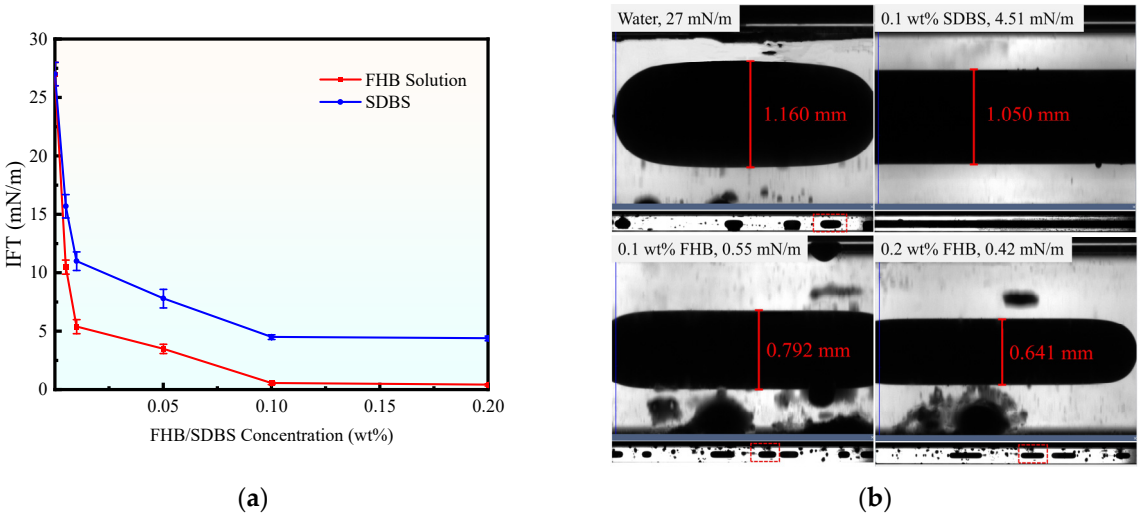


Figure 14. (**a**) IFT measurement results in different media; (**b**) IFT measurement result images.

3.6. Oil Displacement Performance

3.6.1. Core Flooding Tests

Based on the confirmed ability of the FHB system to significantly alter rock surface wettability and oil-water interfacial properties, systematic core flooding experiments were conducted to further validate its oil displacement performance within actual reservoir porous media. Natural low-permeability cores from the Daqing Oilfield (average per-

meability 8 mD) were used to simulate real reservoir conditions. The water flooding experiments employed a constant injection rate of 0.2 mL/min.

The results (Figure 15) show that during the primary water flooding stage, the injection pressure first increased and then decreased, reaching a maximum of 0.96 MPa. This pressure decline is primarily attributed to water breakthrough at the production end, establishing a flow channel between the injector and producer. When the water cut exceeded 98%, the primary oil recovery was 42%. Subsequently, after injecting the FHB solution and allowing a 12 h reaction period, a secondary water flood was initiated. A slow, increasing trend in injection pressure was observed, indicating that the injected water was mobilizing residual oil within the pore network. This is mainly due to the FHB modification of the rock interfaces, which promotes the stripping and mobilization of residual oil. Isolated oil droplets coalesce and form continuous oil bank slugs within the pore throats under the drive of the injected water. Combined with oil-water viscosity differences and the Jamin effect, this leads to a slight rise in displacement pressure. The decrease in water cut at the outlet concurrently increased the recovery factor, with the secondary water flood achieving a final recovery of 53%, representing an increase of 11%. These experiments demonstrate that modifying the surface properties of core pores via the fluorinated interfacial modifier is a viable strategy for mobilizing and displacing residual oil, leading to a significant enhancement in recovery.

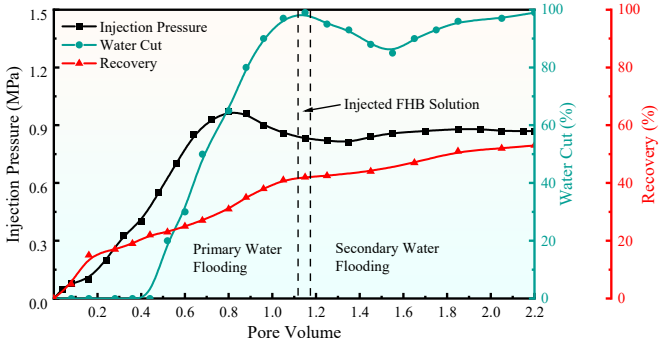


Figure 15. Injection pressure, water cut, and recovery variations during core flooding.

Results from multiple core flooding experiments using similar cores and a permeability gradient series (Table 4) indicate that tighter (lower permeability) cores experience a more pronounced reduction in capillary resistance within pore throats due to wettability alteration, resulting in a greater recovery improvement: the average recovery increase for cores CP-1 to CP-4 was 14%. Among cores CP-5 to CP-8, as permeability increased (indicating less dense rock), the recovery improvement gradually decreased from 17% to 11%.

Table 4. Core flooding test results (multiple groups).

Core No.	Porosity (%)	Permeability (mD)	Equilibrium Displacement Pressure (MPa)	Primary Recovery (%)	Incremental Recovery by EOR (%)
CP-1	16.12	5.23	0.75	38 ± 0.8	14 ± 0.7
CP-2	16.55	7.64	0.83	45 ± 1.1	13 ± 0.5
CP-3	16.10	4.35	0.77	44 ± 1.3	15 ± 0.6
CP-4	15.87	6.08	0.65	40 ± 0.9	14 ± 0.6
CP-5	14.33	2.55	0.73	41 ± 1.0	17 ± 0.8
CP-6	15.69	9.61	0.66	46 ± 1.2	11 ± 0.5
CP-7	17.02	17.34	0.58	43 ± 1.1	12 ± 0.7
CP-8	17.11	29.98	0.59	45 ± 1.2	11 ± 0.5

To further simulate heterogeneous reservoir conditions, a parallel core flooding experiment was conducted using two cores with a permeability contrast ratio of 3.4 (a low-permeability core, LP: 12.9 mD; a high-permeability core, HP: 44.2 mD). The results are shown in Figure 16.

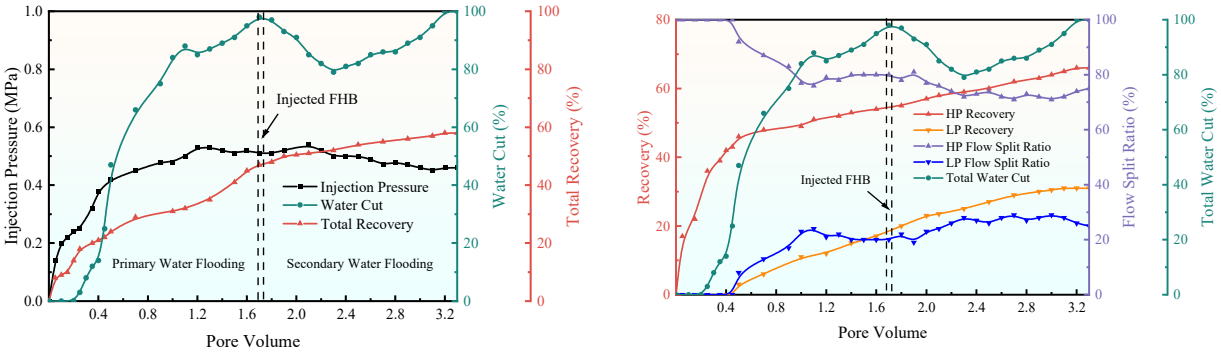


Figure 16. Core flooding performance for heterogeneous parallel cores: (**a**) Overview of parallel core flooding experiment; (**b**) Recovery factor and flow split ratio for the HP and LP cores.

At the equilibrium of the primary water flooding stage, the injection pressure was 0.51 MPa, and the total oil recovery was approximately 48%. After injecting the FHB solution, secondary water flooding yielded an additional 10% increase in total recovery. Specifically, during the primary water flooding, the HP core already achieved a recovery of 55%, primarily because its higher permeability allowed most of the injected water to flow through its dominant flow paths. As injection pressure increased, a small fraction of the injected water began to enter the LP core, gradually increasing its split flow ratio to 21%, resulting in a recovery of only 20% for the LP core. After the FHB solution was injected, alterations in oil-water interfacial properties and core wettability improved the sweep efficiency to some extent during secondary water flooding: the split flow ratio in the LP core increased to a maximum of 29%, and its recovery rose to 31%. The HP core continued to produce oil, reaching a recovery of 66%. The overall final recovery for both cores reached 58%. The contact and diffusion of FHB at the oil-water interface within the LP core contributed to enhancing the sweep efficiency of the injected water.

To achieve even better production performance, combining FHB with gel polymers for conformance control in the HP core could lead to more thorough exploitation of the remaining oil.

3.6.2. Oil Distribution in Displacement Stages

In low-permeability sandstone systems, the bimodal distribution observed in LF-NMR T_2 spectra clearly reflects the heterogeneity of the pore structure (coexistence of microfractures and large pores) and the distribution of fluids within them. Cores CP-1 and CP-8 were selected as examples to analyze the oil saturation reduction before and after FHB modification in low-permeability and high-permeability cores, respectively. In these cores, movable oil within the fracture system exhibits a significant long-T_2 relaxation peak, while bound oil stored within the micro-pores of the matrix corresponds to a characteristic short-T_2 peak (as shown in Figure 17).

Under initial oil-saturated conditions, all pore spaces in the cores are filled with crude oil, resulting in high-intensity LF-NMR signals distributed across a wide range of relaxation times. After the initial conventional water flooding process, the T_2 spectra show distinct changes: the signal peaks in the long-T_2 regions decrease significantly, and the overall peaks

of the spectra shift slightly to the left. This indicates that oil within the large pore channels is effectively displaced and produced, consequently increasing the relative proportion of residual oil trapped in the small pore throats.

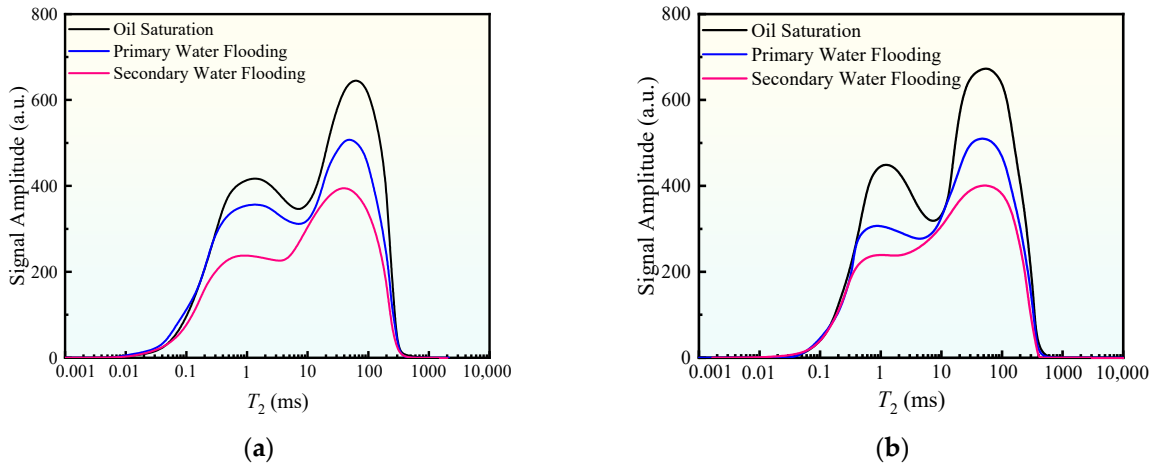


Figure 17. T_2 curves from LF-NMR analysis: (**a**) Core CP-1; (**b**) Core CP-8.

Following the injection of the interfacial modifier and subsequent secondary water flooding, T_2 spectra responses undergo further alteration: signal intensities decrease markedly in both the long-T_2 and short-T_2 regions of each spectrum. These results demonstrate that altering the rock surface wettability via FHB effectively enhances the mobilization of residual oil and improves ultimate oil recovery. Furthermore, the significant reduction in the short-T_2 region signals indicates that contact angle modification is particularly effective for improving oil recovery in low-permeability reservoirs. By significantly reducing the adhesion resistance of both oil and water phases on the pore walls, FHB not only contributes to reducing injection pressure and enhancing injectivity, thereby expanding the effective sweep volume of injected water, but also serves as the core mechanism leading to the further reduction in signal intensity in the short- T_2 regions, which correspond to the domains where residual oil is stored in micro-pore throats.

After integration conversion, the oil distribution results are shown in Figure 18 (initial oil saturation is set as 100%). In the initial oil-saturated state, the oil content in the 4–20 μm pores of core CP-1 was 62.2%, while that of core CP-8 was 54.7%. No oil signal was detected in pores larger than 20 μm in either core, indicating the selected cores contain virtually no pore throats exceeding 20 μm.

After the primary water flooding, the oil content in the 4–8 μm pores of CP-1 decreased from 42.8% to 26.7%, and the remaining oil in the 8–20 μm pores decreased from 19.4% to 7.6%. The significant reduction in both intervals indicates that most of the oil in these ranges was displaced, with some residual oil remaining trapped in the 4–8 μm pore throats. In core CP-8, the oil in the 8–20 μm pores decreased from 27.0% to 21.7%, and the oil content in the 4–8 μm pores decreased from 27.7% to 23.3%. Due to the oil-water viscosity contrast, the injected water formed preferential flow paths through the larger, well-connected pores, making it difficult to enter other less-connected pores, resulting in a relatively smaller reduction in oil content within the 4–8 μm pores. Furthermore, the displacement efficiency in the micro-pores (0.4–4 μm) was very limited. In core CP-1, the oil content in this interval increased slightly from 34.3% to 36.0%, as the injected water's sweep pushed some oil from larger pores into smaller throats. In core CP-8, it decreased slightly from 43.3% to 40.0%. Overall, it is evident that a considerable amount of residual oil remained in both cores after

initial flooding, necessitating methods to enhance injection efficiency and mobilize this residual oil for further recovery improvement.

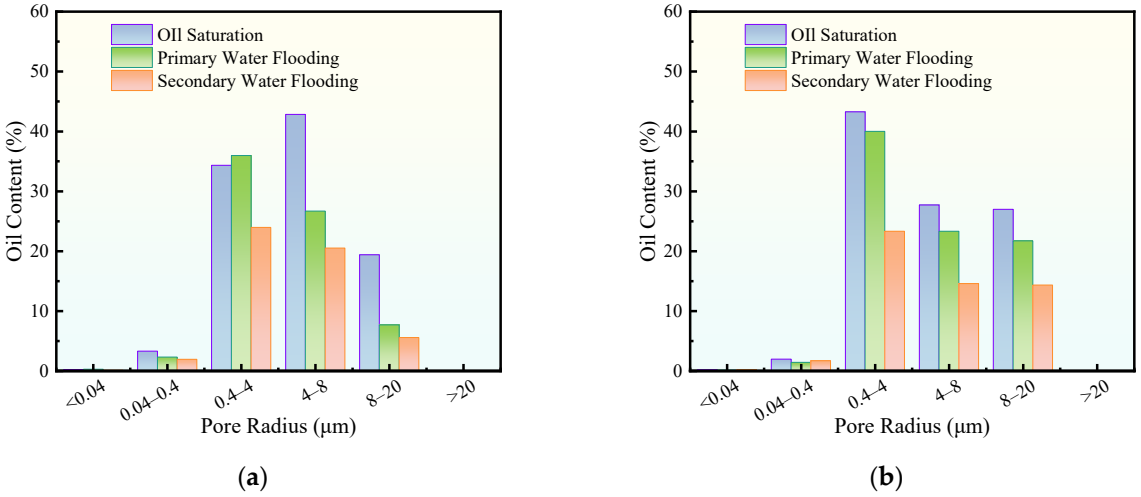


Figure 18. Oil distribution in cores after different displacement stages: (**a**) Core CP-1; (**b**) Core CP-8.

After the injection of FHB, oil production at the outlet increased again. Specifically, the oil content in pores larger than 4 μm decreased further: by 8.3% in CP-1 and by 16.2% in CP-8. More importantly, significant displacement of residual oil occurred within the small pores (0.4–4 μm). The oil content in this interval decreased from 36.0% to 23.9% in CP-1, and from 40.0% to 23.3% in CP-8. These LF-NMR results, which directly quantify the distribution of residual oil signals within different pore sizes in the cores, provide clear evidence that FHB, functioning as a chemical agent capable of wettability alteration, IFT reduction, and injectivity improvement, possesses excellent EOR performance.

3.6.3. Oil-Water Flowability Analysis

This study further investigated the impact of altered core pore surface wettability on oil-water flow efficiency. Two low-permeability cores (10 mD each) were used: one served as a control, saturated with formation water and oil, aged, and then water-flooded while displacement parameters were recorded; the other was saturated to a similar initial oil saturation, aged, and flooded using an FHB solution as a preflush. Data from both processes were compared by recording effluent flow rates and displacement pressures, plotting the relative permeability curves for cores before and after modification (Figure 19; K_{ro}, K_{rw}, and S_w denote oil relative permeability, water relative permeability, and water saturation, respectively).

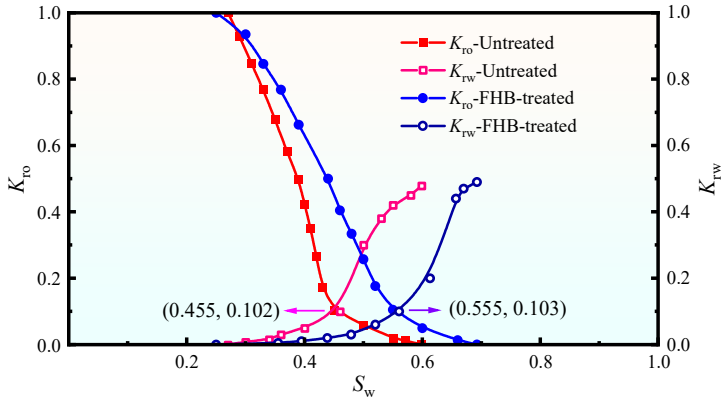


Figure 19. Oil-water relative permeability curves for cores before and after FHB treatment.

Results show that in the untreated core, the initial oil saturation was 0.73, declining to a residual oil saturation of 0.40 after water flooding, yielding a recovery rate of 45%. The two-phase flow region occurred at water saturations between 0.27 and 0.60. In the FHB-treated core, oil saturation decreased from 0.75 to 0.31, achieving a recovery rate of 58%, with the two-phase flow region extending from S_w = 0.25 to 0.69. During water flooding, as water saturation increased, the oil relative permeability decreased slowly initially and then rapidly, while water relative permeability exhibited accelerated growth. This is because oil initially occupied the main flow paths in pore centers; at low water cuts, injected water had limited ability to displace oil in continuous paths. As water saturation rose, water formed continuous channels, displacing oil into smaller pores or isolating it into droplets (Jamin effect), disrupting oil continuity, increasing flow resistance, and causing oil permeability to drop rapidly as water permeability rose [35].

The FHB-treated core exhibited a broader two-phase flow region, indicating that FHB modification improved wettability, allowing fluids to flow more smoothly and enabling oil and water to coexist and flow over a wider saturation range. This delayed early water breakthrough, sustained oil displacement toward production wells, enhanced recovery, and provided greater operational flexibility for adjusting production strategies (e.g., injection rate or well pattern optimization). In contrast, the untreated core, with its oil-wet surface and high capillary resistance, was difficult to inject into, leaving significant residual oil unmobilized. Additionally, the equal-permeability point (where $K_{ro} = K_{rw}$) shifted from S_w = 0.455 to 0.555 after FHB treatment, indicating reduced oil-wettability. This delays water breakthrough and slows water cut rise at the producer, which is crucial for maximizing reservoir potential and improving ultimate recovery.

3.6.4. Water Film Thickness Reduction

The flow efficiency of fluids in core pores is often related to the conductivity of the throats. The bound water film on the pore surfaces, which can be micron-scale, not only occupies flow space but also reduces the efficiency of injected water and limits further recovery improvement through adhesive resistance. Therefore, gas flooding was used to preliminarily determine the thickness of the water film inside the pores before and after FHB modification. Two cores were saturated with formation water under vacuum, after which nitrogen was injected at a constant rate to slowly displace the water. The effluent flow rate and displacement pressure were recorded, and the water film thickness was calculated using Equations (5) and (6). The cores were then resaturated with FHB solution, allowed to react sufficiently, and the gas flooding experiment was repeated to compare the results.

As shown in Table 5, after FHB treatment, the flow of the water phase in the pores was significantly improved. The gas-measured equilibrium permeability of core CF01 increased by 23.2% (from 14.73 mD to 18.15 mD), while that of CF02 increased by 46.0% (from 3.24 mD to 6.00 mD). This is primarily because after FHB modification, the core surface becomes hydrophobic, reducing the adhesive resistance of water in the throats and promoting its mobility. The smaller the pore radius, the greater the impact of reduced capillary resistance; thus, the effect is more pronounced in tighter cores, resulting in a more significant permeability improvement. Furthermore, after FHB modification, the average displacement pressure decreased by 0.06 MPa for CF01 and 0.11 MPa for CF02. As fluid mobility within the pores is enhanced, this manifests as a reduction in displacement pressure at the injection end. Finally, further calculations revealed that the reduction in bound water film thickness is the primary mechanism behind the pressure reduction and injectivity improvement achieved by FHB. By grafting hydrophobic-oleophobic fluorocarbon chains onto the rock surface, FHB reduces the proportion of immobile water in the pore throats: the water film

thickness decreased by 31.3% in CF01 and 31.6% in CF02. This enhances flow efficiency during displacement, reduces ineffective water cycling, expands the sweep efficiency of water flooding, and ultimately promotes increased oil recovery.

Table 5. Comparison of core parameters before and after FHB treatment.

Core No.	Porosity (%)	Core Stage	Equilibrium Permeability (mD)	Equilibrium Displacement Pressure (MPa)	Average Water Film Thickness (μm)
CF01	16.68	Untreated	14.73	0.54	2.59 ± 0.03
		FHB-treated	18.15	0.48	1.78 ± 0.02
CF02	14.25	Untreated	3.24	0.62	1.17 ± 0.01
		FHB-treated	6.00	0.51	0.80 ± 0.01

3.7. Field Application Results and Economic Analysis

Based on laboratory experiments confirming the significant effectiveness of the FHB solution system in improving rock surface properties, reducing oil-water IFT, decreasing bound water film thickness, lowering injection pressure, and enhancing oil recovery, a field trial was conducted in a low-production well in the Daqing Oilfield to further verify its applicability under complex actual reservoir conditions. Utilizing a huff-and-puff alternating injection technique, a 2 wt% FHB solution and formation water were injected cyclically. This process both expands the sweep volume of FHB within the formation and allows for its gradual dilution to lower concentrations, ensuring a balance between controllable material costs and effective performance. It is noteworthy that the 2 wt% concentration was not an arbitrary selection but was determined through integrated analysis of reservoir characteristics—including porosity, permeability, and effective thickness—of the target well group. This engineering design ensured an adequate propagation radius and performance of FHB within the heterogeneous formation. As the solution disperses radially from the wellbore, its concentration decreases gradually, interacting with rock surfaces across a broader range and effectively modifying the wettability of the reservoir.

As shown in Figure 20, prior to the treatment implemented in November 2024, the well exhibited an average daily oil production of only 3.1 t/d, coupled with a gradually rising water cut that had reached 68.9%. These conditions indicated insufficient economic benefits and a clear declining production trend. Following the company's plan, a field trial was conducted in November of that year. After injecting 3 m^3 of the FHB solution and displacing it deep into the formation using formation water, the well was shut in for a 2-day reaction period. Subsequent water flooding demonstrated a significant production enhancement effect: the average oil production increased to 4.9 t/d, while the water cut at the production end decreased by 13.4 percentage points (from 68.9% to 55.5%). This improvement has been sustained until June 2025, indicating that FHB's modification effect on the reservoir and its ability to enhance oil recovery possess practical application value, showing promise for validation in larger-scale field trials to confirm its broader applicability. It is noteworthy that the application of FHB for EOR is limited in ultra-low permeability reservoirs and shale oil reservoirs where conventional water flooding is not feasible. This limitation is inherent to traditional water flooding as well, because the FHB solution requires water as a carrier to facilitate its diffusion within the formation. Under conditions where injection is completely infeasible, FHB cannot exert its modifying effect on the formation.

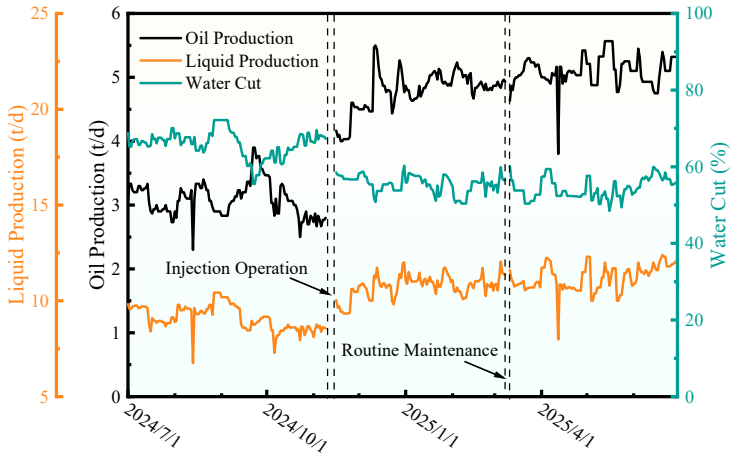


Figure 20. Production data of a test well in Daqing Oilfield.

It is recognized that perfluorinated compounds (PFCs) are persistent organic pollutants, and their environmental impact requires careful evaluation. In this pilot trial, based on the demonstrated stability and anti-aging properties of the FHB-treated rock, it is anticipated that the majority of the injected FHB will be immobilized onto the rock surface through chemisorption, leading to a progressive decrease in its concentration in the formation water. For future large-scale applications, a comprehensive monitoring program would be essential. This would include systematic sampling and analysis of fluorine content in produced water to track potential environmental release. Additionally, implementation of a closed-loop management strategy, where produced water is reinjected into the formation, would be crucial to minimize environmental discharge. Although the current field trial received approval from the operating company's experts, the principles of green and sustainable development remain central to our ongoing research. Future studies in fluorinated chemistry for enhanced oil recovery will explicitly incorporate comprehensive environmental safety assessments as a core component of the evaluation process.

Given that the synthesis process for the perfluorinated compounds used in this study involves higher costs compared to traditional ionic surfactants, a preliminary economic assessment (considering only material costs) of mature EOR technologies was conducted alongside this field trial. As seen in Table 6, the market price of fluorocarbon FHB is approximately 2000 k RMB/t. The injected FHB solution concentration was 2%, injected alternately with formation water. The single-well cost for using 3 tons of FHB is about 120 k RMB. For comparison, the typical dosage range for petroleum sulfonate is 0.25–0.5% [36]. With an injection volume of 200 tons and a market price of 120 k RMB/t, the single-well injection cost for petroleum sulfonate would be approximately 60–120 k RMB. Hydrophobically associating HPAM polymers require larger injection volumes depending on the specific conditions. Assuming an injection volume of 600 tons of a 1600 mg/L polymer solution [37] and a market price of 30 k RMB/t, the single-well cost would be approximately 28.8 k RMB. For hydrophobic nano-silica, with an injection volume of 200 tons and a required concentration of 0.1–0.5% [38], the single-well cost ranges from 60 k to 600 k RMB. Although the material cost of FHB is higher than that of polymers, it is lower than that of sulfonate surfactants or hydrophobic nanoparticles, making the overall expenditure controllable. Furthermore, FHB does not face issues like thermal degradation associated with polymers or dispersion stability problems common with nanoparticles. Based on laboratory experiments and field trial data, FHB demonstrates good anti-aging performance and sustains production enhancement for an extended period without the need for repeated chemical replenishment, thereby

saving costs associated with repeated well shutdowns for treatments. With longer-term observation, its comprehensive cost may potentially be lower than other EOR techniques.

Table 6. Cost comparison of chemical EOR technologies and materials.

Chemical	Concentration	Dosage (t)	Price (RMB/t)	Cost (RMB/Well)	Note
FHB	2%	3	2000 k	120 k	No continuous injection required
Sulfonates	0.25–0.5%	0.5–1	120 k	60 k–120 k	Concentration maintenance required
HPAM Polymer	1600 mg/L	0.96	30 k	28.8 k	
Nano-SiO_2	0.1–0.5%	0.2–1	300 k	60–300 k	

4. Conclusions

This study systematically investigated the fluorinated interfacial modifier FHB for EOR, demonstrating its effectiveness through laboratory experiments and a successful field trial. The main conclusions are as follows:

1. Characterization via NMR, FT-IR, XPS, SEM, and EDS confirmed the successful synthesis of FHB and its chemical grafting onto the core surface, significantly altering surface properties.
2. Treatment with a 0.1 wt% FHB solution at 55 °C increased the water and oil contact angles on the core surface to 136° and 117°, respectively, achieving effective hydrophobicity and oleophobicity. TGA and aging tests confirmed the stability of this modification due to robust chemical bonding.
3. FHB grafting significantly reduced capillary resistance in spontaneous imbibition tests, lowered the surface free energy and adhesion work of fluids, and decreased oil-water IFT from 27 mN/m to 0.55 mN/m, thereby enhancing fluid mobility and residual oil mobilization.
4. Core flooding experiments showed an increase in total oil recovery from 42% to 53% after FHB treatment. LF-NMR confirmed reduced residual oil saturation across various pore sizes. Relative permeability curves indicated a delayed equal-permeability point, and gas displacement tests measured a reduced bound water film thickness, collectively demonstrating improved flow dynamics and injection efficiency.
5. A field trial in a Daqing Oilfield well increased oil production by 1.8 t/d, sustaining this gain for months. A preliminary economic analysis supports the cost-effectiveness of FHB for EOR, highlighting its practical potential.

Author Contributions: Conceptualization, R.L. and X.Y.; methodology, H.L. and H.S.; validation, R.L., X.G., F.Z. and H.S.; formal analysis, Z.L.; investigation, L.H. and W.S.; writing—original draft, R.L.; writing—review and editing, H.L. and X.Y.; supervision, H.S.; project administration, H.L. All authors have read and agreed to the published version of the manuscript.

Funding: This research received no external funding.

Data Availability Statement: Data are available upon reasonable request to the corresponding author due to privacy.

Acknowledgments: The authors sincerely acknowledge the support from the State Key Laboratory of Oil and Gas Reservoir Geology and Exploitation and the College of Energy at Chengdu University of Technology for providing advanced experimental platforms. We also extend our thanks to all co-authors for their collaboration, as well as to the Daqing Oilfield Company (PetroChina) for their valuable technical and operational support during the field trial.

Conflicts of Interest: Zhe Li and Huaqiang Shi were employed by PetroChina Changqing Oilfield Company. The remaining authors declare that the research was conducted in the absence of any commercial or financial relationships that could be construed as a potential conflict of interest.

Abbreviations

The following abbreviations are used in this manuscript:

LF-NMR	Low Field Nuclear Magnetic Resonance
XPS	X-ray Photoelectron Spectroscopy
IFT	Interfacial Tension
EOR	Enhanced Oil Recovery

Appendix A

Static Adsorption Experiment

The static adsorption experiments provided critical insights into the interaction mechanism of FHB on the rock surface through analysis of adsorption kinetics and isotherms. The conformity of the adsorption process with the pseudo-second-order kinetic model indicates that it is governed by chemisorption. Meanwhile, the agreement of the adsorption isotherm with the Langmuir monolayer model demonstrates that FHB molecules form a tightly packed monolayer on the rock surface via chemical bonding. The combination of chemisorption and monolayer coverage fundamentally ensures the stability and durability of the surface modification layer. Therefore, static adsorption experiments were conducted to thoroughly investigate the modification mechanism of FHB on the rock surface.

The FHB solution used for treating rock powder was prepared in formation water using ethanol as a cosolvent. The concentration of FHB before and after adsorption was determined by high-performance liquid chromatography–mass spectrometry (HPLC-MS). Due to the perfluoroalkyl tail of FHB being not only hydrophobic but also extremely difficult to ionize, it tends to adsorb strongly to reversed-phase C18 columns, which may result in poor chromatographic behavior and compromise quantitative accuracy and precision. To address this, the residual liquid after reaction was subjected to hydrolysis under strong alkaline conditions, followed by high-temperature reflux and acidification, to completely convert FHB into perfluoroalkyl acid (as shown in Figure A1; the molar ratio of the resulting perfluoroalkyl acid to FHB is 1:1). This process enables effective chromatographic separation and mass spectrometric ionization.



Figure A1. Stoichiometric relationship between perfluoroalkyl acid and FHB.

Standard solutions at concentrations of 226.7 mg/L, 600.8 mg/L, 1398.0 mg/L, 2192.5 mg/L, 3354.5 mg/L, and 4597.1 mg/L were prepared using a perfluoroalkyl acid standard (Sigma-Aldrich, analytical grade) dissolved in formation water. Formation water was used as the blank to correct for background interference. A standard curve (Figure A2) was constructed by plotting chromatographic peak area against concentration, yielding the regression equation $Y = 321.37X - 8567.86$ with a correlation coefficient (R^2) of 0.99984.

The sandstone samples were ground and sieved to obtain 100-mesh particles, which were then cleaned and dried. Subsequently, 1.0 g of the prepared sandstone particles was placed into a series of centrifuge tubes. According to a solid-to-liquid ratio of 1:20, a 1000 mg/L FHB solution was added to each tube. The mixtures were fully reacted under constant temperature oscillation at 55 °C. At predetermined intervals, the solid and liquid

phases were separated using a centrifuge. A small amount of the supernatant was collected to measure the residual FHB concentration. The difference in FHB concentration before and after adsorption was determined by HPLC–MS, and the adsorption capacity was calculated based on mass balance (Equation (A1)):

$$q_t = \frac{(C_0 - C_t)}{m} \times V \quad \text{(A1)}$$

where q_t is the adsorption capacity at time t (mg/g), C_0 is the initial concentration of FHB (mg/L), C_t is the residual concentration at time t (mg/L), V is the volume of the solution (L), and m is the mass of sandstone (g). Adsorption equilibrium was considered to be reached when C_t no longer changed, at which point the corresponding equilibrium adsorption capacity was determined.

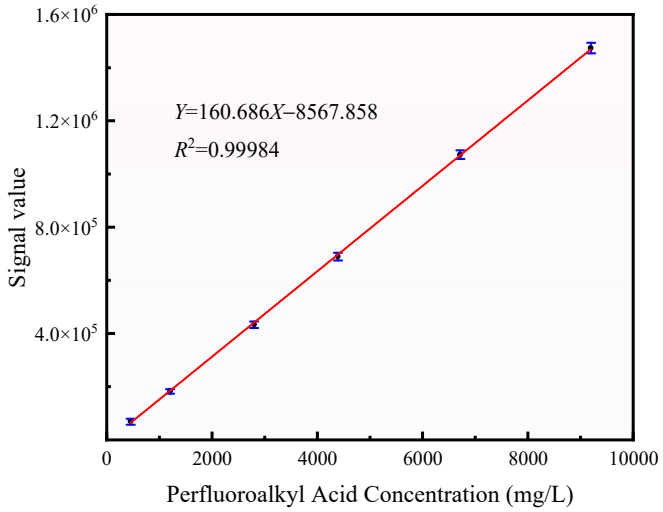


Figure A2. Liquid chromatography standard curve for perfluoroalkyl acid.

To investigate the adsorption rate and the controlling steps of FHB adsorption, the adsorption capacity–time data were nonlinearly fitted using the pseudo-first-order and pseudo-second-order kinetic models. The pseudo-first-order model is based on the assumption that the adsorption rate is dominated by physical diffusion processes, as shown in Equation (A2):

$$\ln(q_e - q_t) = \ln q_e - k_1 t \quad \text{(A2)}$$

where q_t is the adsorption capacity at time t (mg/g), q_e is the theoretical equilibrium adsorption capacity (mg/g), and k_1 is the pseudo-first-order rate constant (min^{-1}). This model is generally more applicable to the initial stages of adsorption.

The pseudo-second-order model is based on the assumption that the adsorption rate is controlled by chemisorption mechanisms, meaning the adsorption rate of FHB is proportional to the square of the number of unoccupied active sites on the rock surface, as expressed by Equation (A3):

$$\frac{t}{q_t} = \frac{1}{k_2 q_e^2} + \frac{t}{q_e} \quad \text{(A3)}$$

where k_2 is the pseudo-second-order rate constant (g/(mg·min)). This model can be used to indicate the presence of chemical bonding between the adsorbate (FHB) and the adsorbent (rock surface).

To further clarify the adsorption pattern of FHB on the rock surface, the batch adsorption data obtained at 55 °C after reaching equilibrium were fitted using the Langmuir and Freundlich isotherm models (Equations (A4) and (A5), respectively). The Langmuir

model is based on the ideal assumption of monomolecular-layer chemisorption, where the adsorbent surface is considered uniform in energy, each active site can adsorb only one molecule, and there are no interactions between adsorbed molecules. The Freundlich model, in contrast, is an empirical equation suitable for describing multilayer adsorption on heterogeneous surfaces under non-ideal conditions.

$$\frac{C_e}{q_e} = \frac{1}{K_L q_{\max}} + \frac{C_e}{q_{\max}} \tag{A4}$$

where C_e (mg/L) is the equilibrium concentration in solution, q_e (mg/g) is the equilibrium adsorption capacity, $q_{\max}$ (mg/g) is the theoretical maximum adsorption capacity representing the amount required to form a complete monolayer, and K_L (L/mg) is the Langmuir constant related to the adsorption binding energy. A value of R^2 closer to 1 indicates that the adsorption process of FHB on the rock surface better conforms to monolayer adsorption characteristics.

$$\ln q_e = \ln K_F + \frac{1}{n} \ln C_e \tag{A5}$$

where KF is the Freundlich constant, roughly representing the adsorption capacity ((mg/g)/(L/mg)$^{1/n}$), and $1/n$ is the heterogeneity factor, characterizing the adsorption intensity and surface heterogeneity. When $0.1 < 1/n < 0.5$, the adsorption process is considered favorable. By fitting the isotherm models, it is possible to determine whether the arrangement of FHB molecules on the rock surface is a dense monolayer or a loose multilayer, which is crucial for evaluating the stability of the modification layer.

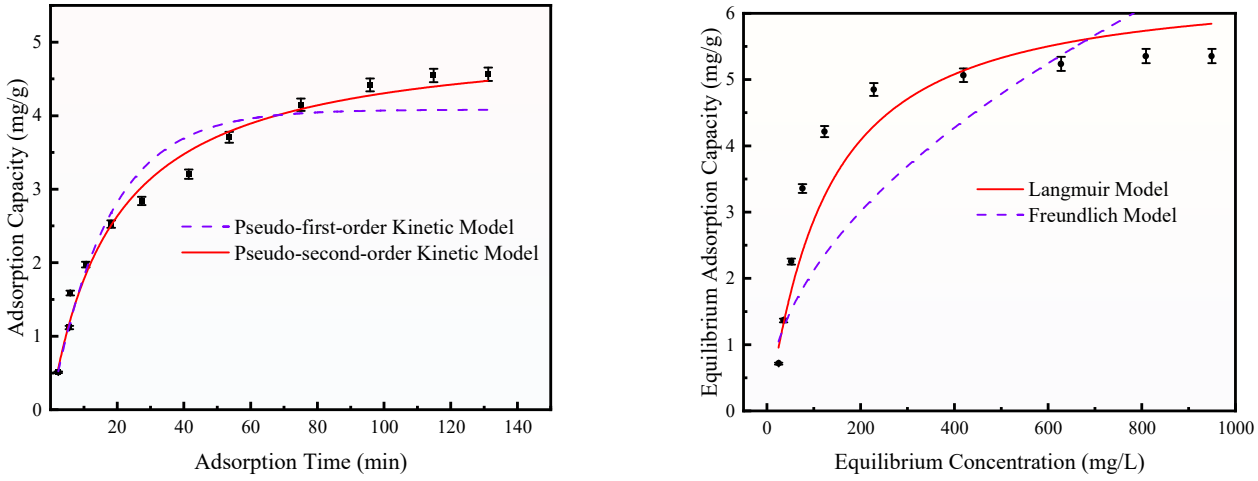
The sandstone is primarily composed of quartz (SiO_2) and feldspar, with surfaces rich in hydroxyl groups (–OH). The FHB molecule contains siloxane groups (–Si(OCH$_3$)$_3$), which can undergo a silanization condensation reaction with the –OH groups on the sandstone surface. The resulting Si–O–Si covalent bond with the sandstone exhibits high bond energy (~360 kJ/mol), imparting irreversibility and resistance to flushing. In contrast, conventional surfactants and modified nanoparticles are retained on rock pore surfaces mainly through physical adsorption mediated by van der Waals forces (bond energy ~0.1–10 kJ/mol), which is prone to desorption and exhibits poor stability. By quantitatively analyzing the adsorption behavior of FHB on the sandstone surface, we aim to assist in verifying the adsorption type (physical/chemical) of FHB and further substantiate the stability of its action on the rock surface.

The relationship between the adsorption capacity of FHB on the rock surface and adsorption time at a formation temperature of 55 °C is shown in Figure A3a. The results indicate that the adsorption kinetics of FHB exhibit distinct two-stage characteristics: in the initial stage (0–80 min), the adsorption rate is relatively fast, which is primarily attributed to the abundant hydroxyl active sites on the rock surface providing sufficient adsorption points for FHB molecules; in the later stage (after 80 min), the adsorption rate slows down significantly, as the available surface adsorption sites become progressively occupied and approach saturation. The experimental data were fitted using the pseudo-first-order and pseudo-second-order kinetic models (Table A1). It was found that the pseudo-second-order model better describes the adsorption process of FHB (R^2 = 0.983), yielding a calculated equilibrium adsorption capacity of approximately 5.12 mg/g. The high goodness-of-fit of the pseudo-second-order model indicates that the adsorption rate of FHB on the rock surface is predominantly controlled by chemisorption mechanisms. This suggests that FHB molecules likely combine with active sites on the rock surface through relatively strong chemical bonding, with the adsorption rate being proportional to the square of the number of unoccupied adsorption sites. This result verifies that FHB is anchored to the rock surface via reliable chemical grafting, laying the foundation for the stability of its modification effect.

Table A1. Parameters of the kinetic model fitting for FHB adsorption on the rock surface.

Pseudo-First-Order Kinetics			Pseudo-Second-Order Kinetics		
K_1 (min^{-1})	q_e (mg/g)	R^2	K_2 (g/(mg·min))	q_e (mg/g)	R^2
0.059	4.08	0.930	0.010	5.12	0.983

As shown in Figure A3b, the adsorption behavior of FHB was further investigated through isothermal adsorption experiments. The Langmuir model (R^2 = 0.943) demonstrated a significantly better fit than the Freundlich model (R^2 = 0.793), indicating that the adsorption of FHB on the rock surface tends toward homogeneous monolayer adsorption rather than multilayer adsorption. The maximum adsorption capacity obtained from the Langmuir fit was approximately 6.24 mg/g. This characteristic adherence to the Langmuir monolayer model implies that FHB molecules can form a relatively uniform and densely arranged hydrophobic-oleophobic modification layer on the rock pore surface. Furthermore, since chemisorption inherently involves strong bonding, FHB molecules are less likely to desorb from the rock surface. The monolayer adsorption structure is more orderly and compact compared to multilayer adsorption, where the latter (often dominated by weaker physical interactions such as van der Waals forces) involves complex and disordered intermolecular forces within the layers, making it susceptible to desorption or rearrangement under environmental conditions (e.g., long-term aging, fluid flushing). The favorable wetting stability exhibited by FHB-modified rock cores is crucial for long-term applications in oilfield operations.



(**a**) (**b**)

Figure A3. (**a**) Fitting of the kinetic model for FHB adsorption on the rock surface; (**b**) Fitting of the Langmuir and Freundlich models for FHB adsorption on the rock surface.

Additionally, the key parameters obtained from the model fitting, such as the equilibrium adsorption capacity (5.12 mg/g) and the theoretical maximum monolayer adsorption capacity (6.24 mg/g), are of significant practical importance for designing field-scale treatment protocols. These values provide a crucial quantitative basis for calculating the required FHB dosage in the injection fluid. Furthermore, they serve as fundamental inputs for numerical simulations aimed at predicting the effective propagation radius of FHB within the formation. This enables a more scientific and reliable design for the field application, ensuring effective coverage and long-term stability of the treatment.

References

1. Eleyan, M.I.A.; Çatık, A.N.; Balcılar, M.; Ballı, E. Are long-run income and price elasticities of oil demand time-varying? New evidence from BRICS countries. *Energy* **2021**, *229*, 120710.
2. Hu, D.; Zhao, Y. Outlook for global oil demand in the post-COVID-19 era. In *Annual Report on China's Petroleum, Gas and New Energy Industry (2022–2023)*; Springer Nature: Singapore, 2024; pp. 93–105.
3. Ji, B.; Fang, J. An overview of efficient development practices at low permeability sandstone reservoirs in China. *Energy Geosci.* **2023**, *4*, 100179. [CrossRef]
4. Zhao, M.; Xie, Y.; Li, L.; Dai, C.; Xu, Z.; Dong, Y.; Zeng, H. Nanofluids with superhydrophobic nanoparticles for improved depressurization mechanism in low permeability reservoirs. *Chem. Eng. J.* **2024**, *495*, 153467. [CrossRef]
5. Wang, X.; Zeng, J.; Liu, B.; Zhao, W.; Shi, K.; Jia, K. Insights into the wetting mechanisms in low-permeability sandstone reservoirs and its evolution processes: The shahejie formation in the Dongying Depression, Bohai Bay basin. *Mar. Pet. Geol.* **2025**, *171*, 107179. [CrossRef]
6. Wu, H.; Zhang, N.; Lou, Y.; Zhai, X.; Liu, B.; Li, S. Optimization of fracturing technology for unconventional dense oil reservoirs based on rock brittleness index. *Sci. Rep.* **2024**, *14*, 15214. [CrossRef]
7. Song, H.; Ghosh, P.; Bowers, A.; Niu, F.; Mohanty, K. Low-salinity polymer flood for enhanced oil recovery in low-permeability carbonates. *SPE J.* **2024**, *29*, 443–454. [CrossRef]
8. Yu, H.; Yang, J.; Li, W.; Luo, W.; Kang, H. Study on fluid phase behavior characteristics of low permeability reservoir under different CO_2 injection amounts. *Energy Rep.* **2024**, *12*, 2297–2305. [CrossRef]
9. Haroun, M.; Meng, W.; Rahman, M.M.; Al Kobaisi, M.; Ponnambathayil, J.A.; Suboyin, A.; Ghosh, B. Uncovering smart water flooding mechanisms in carbonate reservoir rocks by integrating the impact of zeta potential on wettability alteration. *Arab. J. Sci. Eng.* **2023**, *48*, 16655–16667. [CrossRef]
10. Grainger, D.W.; Stewart, C.W. Fluorinated coatings and films: Motivation and significance. *ACS Symp. Ser.* **2001**, *787*, 1–14.
11. Liu, X.; Kang, Y.; Yan, L.; Tian, J.; Li, J.; You, L. Implication of interfacial tension reduction and wettability alteration by surfactant on enhanced oil recovery in tight oil reservoirs. *Energy Rep.* **2022**, *8*, 13672–13681. [CrossRef]
12. Al-Amodi, A.O.; Al-Mubaiyedh, U.A.; Sultan, A.S.; Kamal, M.S.; Hussein, I.A. Novel fluorinated surfactants for enhanced oil recovery in carbonate reservoirs. *Can. J. Chem. Eng.* **2016**, *94*, 454–460. [CrossRef]
13. Ilyushin, Y.; Nosova, V.; Krauze, A. Application of Systems Analysis Methods to Construct a Virtual Model of the Field. *Energies* **2025**, *18*, 1012. [CrossRef]
14. Çıtak, A.; Yarbaş, T. Using contact angle measurement technique for determination of the surface free energy of B-SBA-15-x materials. *Int. J. Adhes. Adhes.* **2022**, *112*, 103024. [CrossRef]
15. Chen, M.; Wu, L.; Li, Z. Synthesis of fluoroalkylsilane-coupling agents and their self-assembled monolayers. *Chem. Pap.* **2019**, *73*, 2551–2562. [CrossRef]
16. Haynes, W.M. *CRC Handbook of Chemistry and Physics*, 97th ed.; CRC Press: Boca Raton, FL, USA, 2016.
17. Georgiev, G.A.; Baluschev, S.; Eftimov, P.; Bacheva, M.; Landfester, K. Addressing the apparent controversies between the contact angle-based models for estimation of surface free energy: A critical review. *Colloids Interfaces* **2024**, *8*, 62. [CrossRef]
18. Zamora, J.M.; Marquez, R.; Forgiarini, A.M.; Langevin, D.; Salager, J.L. Interfacial rheology of low interfacial tension systems using a new oscillating spinning drop method. *J. Colloid. Interface Sci.* **2018**, *519*, 27–37. [CrossRef]
19. *GB/T 29172-2012*; Practices for Core Analysis. General Administration of Quality Supervision, Inspection and Quarantine: Beijing, China, 2012.
20. *GB/T 28912-2012*; Test Method for Two-Phase Relative Permeability in Rock. General Administration of Quality Supervision, Inspection and Quarantine: Beijing, China, 2012.
21. Zhang, Y.; Li, H.; He, G.; Tao, Y.; Fu, H. Effect of interface modification of antihypertensive enhancer on water film thickness in core pore. *Oilfield Chem.* **2021**, *38*, 64–67.
22. Liang, B.; Jiang, H.; Li, J.; Gong, C.; Jiang, R.; Qu, S.; Pei, Y.; Yang, H. Investigation of oil saturation development behind spontaneous imbibition front using nuclear magnetic resonance T2. *Energy Fuels* **2017**, *31*, 473–481. [CrossRef]
23. Zhao, G.; Cheng, L.; Jia, P.; Liu, Y.; Feng, H.; Kuang, T.; Wang, Q. Initial occurrence state and movability evaluation of the gulong shale oil reservoir, Songliao basin. *Energies* **2024**, *17*, 1358. [CrossRef]
24. Gong, Y.; Liu, S.; Zhao, M.; Xie, H.; Liu, K. Characterization of micro pore throat radius distribution in tight oil reservoirs by NMR and high pressure mercury injection. *Pet. Geol. Exp.* **2016**, *38*, 389–394.
25. Martins, F.A.; Freitas, M.P. The fluorine gauche effect and a comparison with other halogens in 2-Halofluoroethanes and 2-Haloethanols. *Eur. J. Org. Chem.* **2019**, *2019*, 6401–6406. [CrossRef]
26. Neuman, R.C., Jr.; Rahm, M.L. Synthesis and nuclear magnetic resonance spectra of some 1-Halo-1-iodoalkanes. *J. Org. Chem.* **1966**, *31*, 1857–1859. [CrossRef]
27. Major, G.H.; Fairley, N.; Sherwood, P.M.A.; Linford, M.R.; Terry, J.; Fernandez, V.; Artyushkova, K. Practical guide for curve fitting in x-ray photoelectron spectroscopy. *J. Vac. Sci. Technol. A* **2020**, *38*, 061203.

28. Jin, J.; Wang, Y.; Ren, J.; Nguyen, A.V.; Nguyen, T.A.H. The effect of fluoropolymer on wettability alteration of sandstone at elevated temperatures. *J. Surfactants Deterg.* **2016**, *19*, 1241–1250. [CrossRef]
29. Ratanpara, A.; Kim, M. Wettability Alteration mechanisms in enhanced oil recovery with surfactants and nanofluids: A review with microfluidic applications. *Energies* **2023**, *16*, 8003. [CrossRef]
30. Hirasakl, G.J. Wettability: Fundamentals and surface forces. *SPE Form. Eval.* **1991**, *6*, 217–226.
31. Thomas, M.M.; Clouse, J.A.; Longo, J.M. Adsorption of organic compounds on carbonate minerals: 1. Model compounds and their influence on mineral wettability. *Chem. Geol.* **1993**, *109*, 201–213. [CrossRef]
32. Somoza, A.; Tafur, N.; Arce, A.; Soto, A. Design and performance analysis of a formulation based on SDBS and ionic liquid for EOR in carbonate reservoirs. *J. Pet. Sci. Eng.* **2022**, *209*, 109856.
33. Zhang, X.; Zhou, Z.; Han, L.; Zhang, Y.; Zhang, Q.; Ma, D.; Ma, W.; Zhang, L.; Zhang, L. Mechanism responsible for the reduction of interfacial tension by extended surfactants. *Colloids Surf. A* **2022**, *634*, 128013. [CrossRef]
34. Zhong, C.; Wang, X.; Zeng, G.; Wu, X. Surface and interfacial activities and wetting behavior for a surfactant containing fluorine and a sulfonic group. *Oilfield Chem.* **2020**, *37*, 701–706.
35. Feng, Q.; Zhang, J.; Wang, S.; Wang, X.; Cui, R.; Wang, D.; Bing, S.; Rui, Z. Unified relative permeability model and waterflooding type curves under different levels of water cut. *J. Pet. Sci. Eng.* **2017**, *154*, 204–216. [CrossRef]
36. Xiong, S.; Liu, X.; Liu, W.; He, Y.; Ruan, X. Petroleum sulfonates as oil displacement agents and application to Gudao Oil Field. *Pet. Sci. Technol.* **2009**, *27*, 357–367. [CrossRef]
37. Yi, F.; Huang, B.; Wang, C.; Tang, X.; Wang, X.; Liu, Q.; Su, Y.; Chen, S.; Wu, X.; Chen, B.; et al. Hydrophobically associating polymers dissolved in seawater for enhanced oil recovery of Bohai Offshore Oilfields. *Molecules* **2022**, *27*, 2744. [CrossRef]
38. He, Y.; Liao, K.; Bai, J.; Fu, L.; Ma, Q.; Zhang, X.; Ren, Z.; Wang, W. Study on a Nonionic surfactant/nanoparticle composite flooding system for enhanced oil recovery. *ACS Omega* **2021**, *6*, 11068–11076. [CrossRef]

Disclaimer/Publisher's Note: The statements, opinions and data contained in all publications are solely those of the individual author(s) and contributor(s) and not of MDPI and/or the editor(s). MDPI and/or the editor(s) disclaim responsibility for any injury to people or property resulting from any ideas, methods, instructions or products referred to in the content.